

REVIEW

$\chi^{(2)}$ cascading phenomena and their applications to all-optical signal processing, mode-locking, pulse compression and solitons

G. I. STEGEMAN, D. J. HAGAN

*Center for Research and Education in Optics and Lasers (CREOL),
University of Central Florida, 4000 Central Florida Blvd, CREOL Bldg,
P.O. Box 162700, Orlando, FL 32816-2700, USA*

L. TORNER

*Polytechnic University of Catalunya, Department of Signal Theory and
Communications, Gran Capitan, s/n Campus Nord D3, P.O.B. 30.002,
08080 Barcelona, Spain*

Received and accepted 22 August 1996

Cascading is the process by which the exchange of energy between optical beams interacting via second order nonlinearities ($\chi^{(2)}$) leads to various effects such as nonlinear phase shifts, the generation of new beams, all-optical transistor action, the formation of soliton-like (solitary) waves, etc. Here we review the fundamentals of the processes and discuss experimental verification of the effects and various related applications.

1. Introduction

Nonlinear optics has traditionally been discussed in terms of second and third order nonlinearities and the effects to which they lead. For example, second order nonlinearities are well-known for phenomena such as frequency conversion, parametric amplification, etc. [1–4]. Typically the goal is to optimize the transfer of power from one frequency to another. Third order nonlinearities, on the other hand, are usually associated with an irradiance-dependent refractive index, four wave mixing, solitons, etc., phenomena in that the beam frequencies are degenerate [2–4]. Although there are third order processes that are used for frequency conversion, for example EFISH (electric field induced second harmonic generation) or THG (third harmonic generation), they are primarily used for material characterization and not for efficient frequency conversion [5]. However, it was recognized in the early stages of nonlinear optics that second order phenomena could effectively contribute to third order nonlinearities, and even lead to the generation of spatial solitary waves [6–9]. In such phenomena the emphasis

is on the amplitude and phase shift of the fundamental beam(s) in a second harmonic interaction. Clearly the physics of the process requires two successive second order processes in order for the net output to be back at the input frequency (ω). This can occur via up-conversion ($\omega + \omega \rightarrow 2\omega$, better known as second harmonic generation (SHG)) followed by down-conversion ($2\omega - \omega \rightarrow \omega$), or via down-conversion ($\omega - \omega \rightarrow 0$, better known as optical rectification) followed by up-conversion ($\omega + 0 \rightarrow \omega$). It is the successive nature of the processes needed to modify the fundamental beam that initially led to the name 'cascading' being applied to this class of effects and to the symbolic representation $\chi^{(2)} : \chi^{(2)}$ as the effects are proportional to $[\chi^{(2)}]^2$.

It is interesting to note that the two key features of 'cascading' had been predicted in the first decade of nonlinear optics. The existence of nonlinear phase shifts in the fundamental beam during SHG was first discussed by Ostrovskii in 1967 and the existence of soliton-like (henceforth called simply solitons) waves due to $\chi^{(2)}$ was predicted in 1974 by Karamzin and Sukhorukov [6, 9]. However, until about 1990 there was no evolution of cascading as defined above as a well-defined field. There were sporadic reports aimed at understanding various aspects of related phenomena, with the focus on frequency conversion efficiency [6, 9–19]. In fact the importance of pulse distortion in SHG due to phase modulation was a popular topic in the 1980s [16–19]. The experimental work, starting in the late 1960s, was concerned primarily with measuring the interference between $\chi^{(3)}$ and $\chi^{(2)}$ -related contributions, invariably far from the SHG wavevector-matching condition $\Delta k = 2k_1 - k_3 = 0$ where k_3 and k_1 are the fundamental and harmonic wavevectors respectively [7, 20–23]. In addition, cascading was used to calibrate the third order susceptibility of glass [24]. In general the resulting cascaded contributions were small because Δk was relatively large and the effective nonlinearity is proportional to $|\chi^{(2)}|^2/\Delta k$. Until recently there was no experiment that definitively showed that cascaded processes could actually be larger or more useful than the corresponding third order effects.

In the late 1980s and early 1990s a number of different experimental developments contributed to the current interest in cascading phenomena. One important factor was two direct experimental measurements of the nonlinear phase shift. A little known Soviet paper by Belashenkov and coworkers reported a nonlinear phase shift of the fundamental in excess of π near the phase-match condition in CDA [25]. A few years later an independent study of nonlinear refraction in a KTP crystal via Z-scan showed a dominant contribution from cascading, again near the phase-matching condition [26]. These experiments showed that cascading was indeed a large effect near phase-matching for SHG. This occurred in a climate in which the nonlinear optics community, especially those interested in all-optical phenomena, had realized that it is extremely difficult to find materials which gave large nonlinear phase shifts via $\chi^{(3)}$ without excessive losses due to one or two photon absorption [27]. However this cascaded nonlinearity is proportional to $|\chi^{(2)}|^2$ and requires phase-matchable geometries to be really useful. Fortunately many new organic materials were being reported in the early 1990s with nonlinearities in the 100s of pm V^{-1} range, for example [28–30]. Furthermore, efficient SHG was being demonstrated with quasi-phase-matching which allowed large, but normally not phase-matchable, $\chi^{(2)}$ coefficients to be used [31]. Cascading offered a new and promising direction to explore for all-optical phenomena.

In a parallel development, the laser community became involved when it was shown experimentally that $\chi^{(2)}$ -active elements in laser cavities could lead to mode-locking and pulse compression [32, 33]. The early 'nonlinear mirror' work of Stankov used a phase-matched SHG crystal and dichroic mirror in a laser cavity to provide positive feedback and amplitude modulation (via SHG conversion) for passive mode-locking and switching [32]. Cerullo and

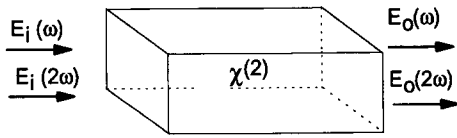


Figure 1 Schematic of the general cascading geometry in which both a fundamental and a second harmonic beam are incident on a $\chi^{(2)}$ -active medium near its phase-matching condition.

coworkers appeared to be the first to use the cascaded nonlinear phase shift away from phase-matching for mode-locking [33].

Coincidentally, there was a growing interest in spatial solitons. Again around 1990 1-D spatial solitons (i.e. beams which diffract in one spatial dimension) were first demonstrated in slab glass waveguides [34]. This has led to the investigation of new spatial solitons in different kinds of materials, which have now included quadratic solitons, photorefractive solitons, Manakov and vector solitons, etc. [35–38]. Cascaded soliton waves were part of this wave of new types of spatial solitons.

Thus, the key elements needed to make cascading an interesting alternative to third order nonlinearities for ‘self-action’ effects were in place by about 1990. As will be discussed here, since then there has been a great deal of progress in the field [39, 40].

What are the distinguishing features of cascading? Consider the generalized SHG geometry shown in Fig. 1. The fundamental beam inside the medium is given by

$$E(\omega) = \frac{1}{2} |a_1(z)| \sqrt{\frac{2}{cne_0}} \exp\{i[\omega t - kz - \phi^{NL}(z)]\} + c. c. \quad (1)$$

There is both a nonlinear phase shift $\phi^{NL}(z)$ and a modulation in the fundamental amplitude distribution $|a_1(z)|$. In the last few years, near phase-matching a number of cascading phenomena based on $\phi^{NL}(z)$ and $|a_1(z)|$ have been investigated:

- (1) large nonlinear phase shifts ($> 2\pi$);
- (2) cavity and integrated waveguide all-optical devices;
- (3) transistor action, i.e. gain and phase modulation;
- (4) applications to lasers for mode-locking, pulse compression, etc.;
- (5) frequency degenerate and almost degenerate four wave mixing;
- (6) spatial soliton waves, their steering and beam transformation.

These have all been demonstrated experimentally. Concurrently a large number of effects based on both the nonlinear phase shift and the formation of soliton waves, including their interactions, have been analysed theoretically. In this paper we will review the simple physics involved in the nonlinear phase shift and soliton formation aspects of cascading, some of the essential features (especially those different from similar third order effects), related phenomena and selected experiments.

2. The nonlinear phase shift via SHG

2.1. Theoretical considerations and physical model

Cascading effects will occur in all parametric interactions governed by the second order nonlinearities $\chi^{(2)}$. This clearly includes SHG, sum and difference frequency generation, optical rectification, optical parametric oscillators and amplifiers, etc. In the most complicated case, the input can include finite cross-section pulsed beams at all of the interacting frequencies with spatial and temporal walk-off between them. Because the relative beam phases at the input are important parameters in such coherent interactions, the response can be very complicated indeed.

There is a rich variety of phenomena which can occur. One way of classifying them is to discuss the effects in terms of the two principal methods of phase-matching used in practice,

Type I and Type II [3]. Note that other techniques such as quasi-phase-matching are now used but for our purposes they can usually be discussed as Type I.

2.1.1. Type I phase-matching

2.1.1.1. Unseeded SHG

In order to obtain an understanding of the underlying physics, we consider first the simplest case of Type I phase-matching (one fundamental input and no input SH) with plane wave inputs (no spatial diffraction, strictly valid for a channel waveguide). The fundamental beam amplitude of the form

$$E(\omega) = \frac{1}{2} a_1(0) \sqrt{\frac{2}{cn\epsilon_0}} \exp[i(\omega t - kz)] + \text{c. c.} \quad (2)$$

is incident onto a lossless $\chi^{(2)}$ -active medium at $z = 0$. The evolution of both the fundamental beam, given by Equation 1 with $a_1(z) = |a_1(z)| \exp[-i\phi^{\text{NL}}(z)]$, and the generated second harmonic $E(2\omega)$ [amplitude $a_3(z)$], is described by

$$\frac{d}{dz} a_1(z) = -i\kappa(-\omega; 2\omega, -\omega) a_3(z) a_1(z) e^{i\Delta kz} \quad (3)$$

$$\frac{d}{dz} a_3(z) = -i\kappa(-2\omega; \omega, \omega) a_1^2(z) e^{-i\Delta kz} \quad (4)$$

$$\kappa(-2\omega; \omega, \omega) = \frac{\omega d_{ijk}^{(2)}(-2\omega; \omega, \omega) e_i(2\omega) e_j(\omega) e_k(\omega)}{[2n_i(2\omega) n_j(\omega) n_k(\omega) c^3 \epsilon_0]^{1/2}} \quad (5)$$

$$\kappa(-\omega; 2\omega, -\omega) = \frac{\omega d_{ijk}^{(2)}(-\omega; 2\omega, -\omega) e_i(\omega) e_j(2\omega) e_k(\omega)}{[2n_i(\omega) n_j(2\omega) n_k(\omega) c^3 \epsilon_0]^{1/2}} \quad (6)$$

for uniform wavevector mismatch $\Delta k = 2k_{\text{vac}}(\omega)[n(\omega) - n(2\omega)]$. When full permutation symmetry is valid, $\kappa(-2\omega; \omega, \omega) = \kappa(-\omega; 2\omega, -\omega) = \kappa$ is the nonlinear coupling coefficient. The electric field polarization vectors are $e(\omega, 2\omega)$. The irradiance (plane wave) is given by $|a_1(z)|^2 = I_1(z)$. All of the nonlinear phase shift physics is contained in the solutions to these equations under different input beam conditions. For SHG, $|a_1(0)|^2 = I_1(0)$ and $|a_3(0)|^2 = I_3(0) = 0$. Analytical solutions were first given by Armstrong *et al.* and the equations have subsequently been analysed for cascading in detail by a number of authors [1, 6, 11, 41–43]. Our approach in discussing the nonlinear phase shifts will be to give some typical results and then offer a simple physical interpretation.

Only under very restrictive conditions is there a linear dependence of ϕ^{NL} on either the distance into the sample or on the incident irradiance (and hence equivalence to $\chi^{(3)}$). An example of the variation of $\phi^{\text{NL}}(z)$ with distance is reproduced in Fig. 2a [41]. This shows a linear variation with distance only for large phase-mismatch $[\Delta kL]$ and/or small phase shifts. In fact the salient characteristic is a stepwise change in $\phi^{\text{NL}}(z)$ with increasing distance, with a maximum step size of $\pi/2$. Note that even for large phase-mismatches the increase occurs via steps, the larger the phase-mismatch the smaller (and more frequent) the steps. Comparison with the throughput curves (Fig. 2b) indicates that the increment in nonlinear phase occurs primarily during the cycle in which power flows back from the harmonic into the fundamental.

The dependence of $\phi^{\text{NL}}(L)$ (i.e. at the output) versus increasing input irradiance is shown in

Fig. 3 [41]. Note that there is an irradiance range over which the nonlinear phase shift is linear in the irradiance. There it is sensible to discuss cascading as leading to an ‘effective third order nonlinearity’ for self-phase modulation, i.e. an ‘effective nonlinear refractive index coefficient $n_{2,\text{eff}}$ ’. It is clear that the maximum phase shift in which this approximation is valid depends on the detuning from phase-matching, the larger the detuning $[\Delta kL]$ the larger the range of irradiances in which this concept is valid. Another feature different from the Kerr nonlinearity case is the apparent saturation of the nonlinear phase shift with irradiance, even after averaging over the steps. In fact $\phi^{\text{NL}}(L)$ becomes asymptotically linear in the field at large phase shifts [41]. This just emphasizes the second order nature of the cascading interaction as being different from the third order nonlinearities in which the effects remain proportional to irradiance unless the material response (and not the process) saturates.

As indicated in Figs 2 and 3, the net phase shift depends on the phase mismatch, commonly called the SHG detuning. This variation is shown in Fig. 4a. Just by adjusting the wavevector mismatch condition, the magnitude and sign of the ‘effective nonlinearity’, i.e. nonlinear phase shift, can be varied. Furthermore there is an irradiance-dependence to the detuning needed for

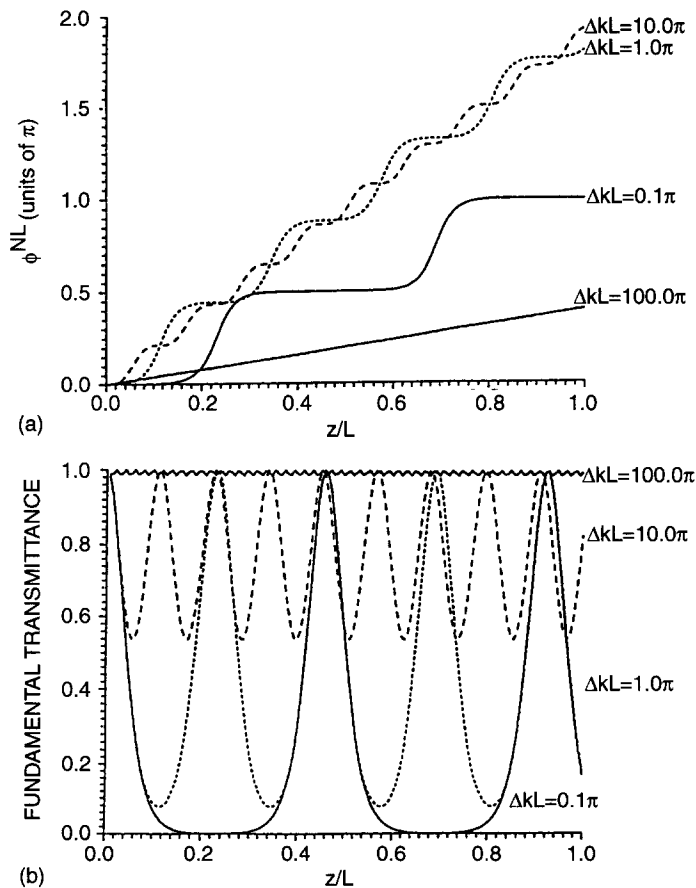


Figure 2 Typical variation of the nonlinear phase shift (a) $\phi^{\text{NL}}(z/L)$ and the transmitted fundamental (b) with normalized distance z/L for various net phase mismatches ΔkL for Type I SHG. (From [41].)

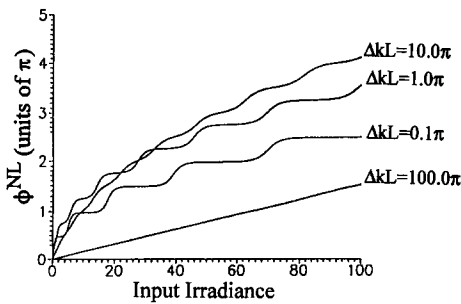


Figure 3 Typical variation in the nonlinear phase shift $\phi^{NL}(L)$ versus fundamental input irradiance for various net phase mismatches. (From [41].)

maximum phase shift: in the small depletion limit, this maximum occurs at $\Delta kL = \pm \pi$. The dispersion in the low depletion limit is reminiscent of the wavelength dispersion in refractive index due to the strong energy exchange between an EM field and a two level transition near resonance: here the corresponding energy exchange is between two electromagnetic modes, the fundamental and second harmonic and the corresponding resonance in the phase-matching condition between the two modes. As shown in Fig. 4b, the ‘price’ for obtaining large phase shifts is effectively the ‘loss’ of the fundamental throughput to second harmonic (which effectively acts as the well-known two photon absorption in $\chi^{(3)}$ nonlinear optics). In fact the connection between the phase shift and the ‘loss’ to SHG has been shown to satisfy the Kramers–Kronig relations in the limit of weak depletion [44]. This reduction in fundamental throughput is a serious drawback for cascading. However, because the process is nonlocal, it can be avoided as will be discussed later. Note also the well-known effective change in coherence length at high input irradiances [1].

There is a simple model which reproduces the essential physics of the nonlinear phase shift and gives useful insights. Off phase-match, the fundamental and harmonic periodically exchange energy with propagation distance. For illustrative purposes, consider the almost phase-matched case in which the fundamental is strongly depleted, $\Delta kL = 0.1\pi$ in Fig. 2. The SH grows with distance from the input, eventually almost completely depleting the fundamental. The part of the fundamental which is not converted to SHG propagates at the phase velocity $v_1 \neq v_3$ where v_3 is the second harmonic phase velocity. After approximately one coherence length, the energy flows from the SH back into the fundamental. During the

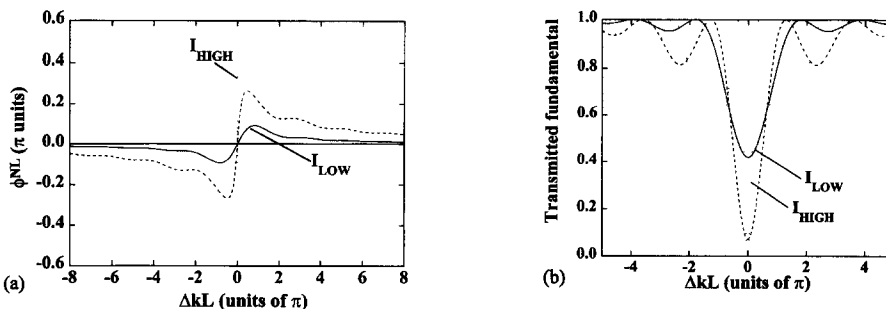


Figure 4 Typical variation in (a) the nonlinear phase shift $\phi^{NL}(L)$ and (b) the fundamental transmission versus detuning from phase matching ΔkL for three different input irradiances. From low to high the parameters correspond to $\kappa = 4$, $L = 1$ and $a_1(0) = 1, 2$ and 4 respectively.

back-conversion cycle of second harmonic to fundamental, the regenerated fundamental wave is no longer in phase with the non-converted fundamental. So the net fundamental phase is either advanced or retarded relative to the unconverted fundamental, depending on which is larger, v_1 or v_3 . The conversion to second harmonic is a nonlinear process and the input fundamental irradiance determines what fraction of the fundamental is converted to SHG. Hence the larger the input irradiance, the larger the contribution from the down-converted fundamental and hence the larger the net nonlinear phase shift. Furthermore, because propagation is involved, this is a nonlocal process, in contrast to $\chi^{(3)}$ based nonlinear phase shifts! Note from Fig. 2 that the upwards step in nonlinear phase does coincide approximately with the back-conversion of the SH to the fundamental. There is also a phase shift produced in the second harmonic. It has been of limited interest to date.

In the limit of negligible fundamental depletion it is possible to give a simple expression for the maximum phase shift and effective nonlinearity $n_{2,\text{eff}}$ which occurs at $\Delta kL = \pm \pi$ [26, 41]:

$$n_{2,\text{eff}} = \pm \frac{4|d_{\text{eff}}^{(2)}|^2 L}{n^3 c \epsilon_0 \lambda} \quad (7)$$

Note that this maximum value is proportional to the sample length. Assuming that phase-matching can be achieved for the coefficients shown, in Table I we list these maximum values.

Given that the largest non-resonant nonlinearity reported to date is $n_2 = 2.2 \times 10^{-12} \text{ cm}^2 \text{ W}^{-1}$ in the single crystal polydiacetylene PTS, clearly cascading offers the promise of very large effective nonlinearities [46].

2.1.1.2. Seeded SHG

The situation becomes considerably more complex when a second harmonic ‘seed’ is included at the input. The fundamental output, both its magnitude and phase, is very sensitive to the relative input phase $\Delta\phi = \phi_3 - 2\phi_1$ between the seed (ϕ_3) and the fundamental (ϕ_1) beams. There are three clear cases here: one, a weak second harmonic seed; two, a strong second harmonic seed; and three, nonlinear eigenmodes.

Trillo, Wabnitz and coworkers have considered the general problem of seeding [47]. They used phase plane portraits of both the fundamental and second harmonic to find the nonlinear eigenmodes, their properties (discussed in detail later) and the regions of instability of the solutions. Using these phase plane portraits, they were able to identify the effects of relative phase angle, seeding power, etc., on the evolution of the fundamental and second harmonic.

TABLE I Effective, optimized, nonlinear coefficients n_2 via cascading for materials with representative d_{ij}

Material $L = 1 \text{ cm}$	d_{ii} (pm V ⁻¹)	d_{ij} (pm V ⁻¹)	n_2 (effective) (cm ² W ⁻¹)
LiNbO ₃	36		2×10^{-11}
LiNbO ₃		5.8	5×10^{-13}
MNA	165		7×10^{-10}
NPP		84	2×10^{-10}
DAST	600		6×10^{-9}

NPP N-(4-Nitrophenyl)-(L)-prolinol [28]

MNA 2-Methyl-4-nitroaniline [45]

DAST Dimethyl amino stilbazolium tosylate [29, 30]

Because the coupled mode equations are in the field and not the irradiance, even a 1% seed in terms of irradiance can produce large effects because it corresponds to a 10% amplitude seed. We give two examples in Figs 5 and 6. In Fig. 5 we show both the fundamental amplitude and nonlinear phase for two different seeding conditions [48]. Clearly large changes occur with very small seed irradiances. In Fig. 6 the detuning curve shows that adding a seed is nearly equivalent to moving the effective phase-matching condition away from $\Delta kL = 0$ [49]. The effect is so large that the fundamental output can be changed from a maximum to a minimum by a π -relative phase change. On the one hand this can be used to implement on-off device functions, on the other hand it also means that the phase is a critical variable requiring sub-wavelength tolerances before the sample. Note that the unseeded case, taken as the limit $I_3(0) \rightarrow 0$, corresponds to $\Delta\phi = -\pi/2$ due to the ‘-i’ in the coupled mode equations, assuming $\phi_1 = 0$ as a reference.

In addition to seeding with SH, a weak fundamental can be used to seed a strong SH. A strong second harmonic input can potentially achieve two goals. Via its coherent interaction with a weak fundamental, the fundamental can be amplified. This case has been analysed by St. J. Russell, and Assanto and coworkers [50, 51]. Alternatively, a large nonlinear phase shift can be induced into the fundamental by copropagating with the strong second harmonic. As suggested by Lefort and Barthelemy, this phase shift could be used to switch an interferometric device [52].

2.1.1.3. Nonlinear eigenmodes

Under appropriate input conditions, a fundamental and harmonic can together form a nonlinear eigenmode. Consider again Equations 2 and 3. For a steady-state solution in which there is no net energy exchange between the fundamental and harmonic, the left-hand side of these equations must be zero. Note that this does not mean that energy (and phase information) is not exchanged, just that the net balance of energy flow is zero. Trillo and Wabnitz, and Kaplan have shown that this leads to two eigenmodes under certain conditions [47, 53]. They must be launched with both a specific difference between their phases at the input, i.e. $\Delta\phi = (S - 1)\pi/2$ with $S = \pm 1$, and with relative wave irradiances given by

$$I(\omega) = 2I(2\omega) + S \frac{c\Delta k}{\omega} \sqrt{I(2\omega)I_{\max}} \quad I_{\max} = \frac{n(\omega)\sqrt{cn(2\omega)\epsilon_0}}{d_{\text{eff}}^{(2)}} \quad (8)$$

As long as $I_{\max} < 4I(2\omega)\omega^2/c^2\Delta k^2$, i.e. for small enough wavevector mismatch, there are two solutions. Otherwise, only the $S = +1$ solution exists. These eigenmodes both have nonlinear

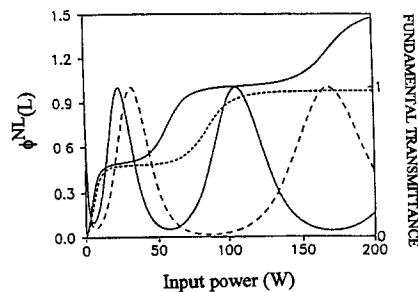


Figure 5 Nonlinear phase shift $\phi^{\text{NL}}(L)$ (monotonically increasing step-like response) and fundamental throughput $P_w(L)/P_w(0)$ (oscillatory response peaking at 1) versus input fundamental power with (solid line) and without (dashed line) a second harmonic input seed power 1000 times smaller than the fundamental for $\Delta kL = 0.1\pi$.

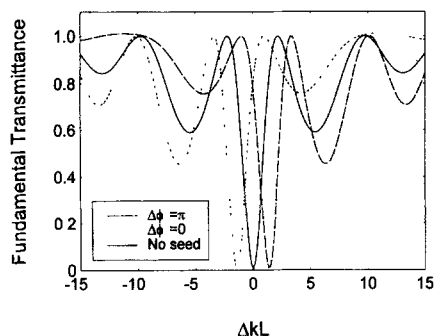


Figure 6 Fundamental transmission versus detuning ΔkL for various relative phase $\Delta\phi = \phi_3 - 2\phi_1$ of the seed second harmonic relative to the fundamental. The seed irradiance is 3.4% of the fundamental (From [49].)

phase shifts which are linear with distance into a medium and field amplitude. They are given by $\phi^{NL}(z) = -S[\omega^2 I(2\omega)/(c^2 I_{max})]^{1/2} z$. It is interesting that the sign of this phase shift depends on the relative phases at the input. However, note that the phase shift is linear in the field, the asymptotic limit of unseeded SHG.

The stability of these cw eigenmodes has proven to be an interesting theoretical question. Kaplan has shown that they are stable against spatial perturbations along the propagation direction in the one-dimensional case, i.e. in planar waveguides. Analysing a different aspect of this problem, Trillo and Ferro have shown that modulational instabilities can occur in the time domain in the presence of perturbations [54]. Frequency sidebands grow around both the fundamental and harmonic frequencies. These latter authors have also considered the stability in the presence of third order nonlinearities and under some conditions chaos was predicted. Their analysis has shown that the eigenmode stability depends on the ratio of the contributions of the two nonlinear processes, cascading and the third order susceptibility.

2.1.2. Type II phase-matching

There are new possibilities (and therefore opportunities) for the case of Type II phase-matching because there are two, independently controlled, fundamental beams [55–61]. This leads to three coupled mode equations for the three complex amplitudes $a_1(z)$ [frequency ω , wavevector k_1], $a_2(z)$ [frequency ω , wavevector k_2] and $a_3(z)$ [frequency 2ω , wavevector k_3]:

$$\frac{d}{dz} a_1(z) = -i\kappa(-\omega; 2\omega, -\omega) a_3(z) a_2^*(z) e^{i\Delta k z} \quad (9)$$

$$\frac{d}{dz} a_2(z) = -i\kappa(-\omega; 2\omega, -\omega) a_1^*(z) a_3(z) e^{i\Delta k z} \quad (10)$$

$$\frac{d}{dz} a_3(z) = -i\kappa(-2\omega; \omega, \omega) a_1(z) a_2(z) e^{-i\Delta k z} \quad (11)$$

where the wavevector mismatch for collinear beams is given by $\Delta k = [k_1 + k_2 - k_3]$ and assuming Kleinmann symmetry again reduces the coupling coefficients to a common κ . The irradiances (plane wave) are given by $I_1(z) = |a_1(z)|^2$, $I_2(z) = |a_2(z)|^2$ and $I_3(z) = |a_3(z)|^2$. For SHG, $|a_1(0)|^2 = I_1(0)$, $|a_2(0)|^2 = I_2(0)$ and $|a_3(0)|^2 = 0$. This case was first analysed by Hutchings *et al.* in the context of sum and difference frequency mixing [55].

The most detailed analytical exposition of this case was given by Kobayakov and colleagues

for Type II SHG [61]. The additional degree of freedom relative to the Type I phase-matching case is the relative irradiance of the two fundamental inputs. (We note that the relative phase of the two input fundamentals does not affect the conversion efficiency or any of the nonlinear phase shifts.) A typical example of the variation in the beam irradiances and nonlinear phase shift versus propagation distance on phase-matching $[\Delta kL]$ is shown in Fig. 7 for the simplest case of phase-matching, $\Delta kL = 0$ [61]. These illustrate some of the major differences from the Type I phase-matching case. The irradiances of all three beams oscillate (Fig. 7) with distance with a period given by

$$L_p(\delta) = \frac{2K[(1 - \delta)/(1 + \delta)]}{\sqrt{1 + \delta}} \quad (12)$$

where $\delta = [I_1(0) - I_2(0)]/[I_1(0) + I_2(0)]$ with $I_1(0) > I_2(0)$ is a measure of the irradiance imbalance. The Manley–Rowe relations require equal energies to be removed from both fundamental beams during SHG and hence the stronger beam only depletes to the point that the weaker beam is completely depleted. For the stronger beam to grow during the succeeding down-conversion cycle, Equation 10 requires a change in sign which can only be accomplished by $a_1(z)$ changing phase by π when its energy increases back from complete depletion. This explains the nonlinear phase shift behaviour for the weak fundamental shown in Fig. 7b. Similarly, the harmonic phase must change by π when the fundamentals pass through a maximum and the harmonic is completely depleted. (Note that [61] has a positive harmonic phase shift because a different form of the coupled mode equations was used there.) The stronger fundamental never can undergo a discontinuous phase change because it never depletes. Note, however, that for exactly equal fundamental irradiances, the response degenerates into that discussed previously for the Type I phase matching case, i.e. the period $L_p \rightarrow \infty$, and there are no nonlinear phase changes in the fundamental. Hence, one expects large changes in the output for a crystal of a given length near irradiance balance when $\delta \rightarrow 0$ with ΔkL small. And indeed this region has been identified as interesting for various optical devices which will be discussed later.

The variation in the nonlinear phase shift of the weak beam as a function of normalized strong beam irradiance is shown in Fig. 8 [59]. Similar to the Type I case, the phase shift becomes linear in the field $[a_1(0)]$ at high irradiances, exhibiting apparent saturation in Fig. 8. The key feature, however, is that the weak beam nonlinear phase shift is optimum when $\delta \rightarrow 1$ whereas the strong beam experiences a small phase shift. Therefore the

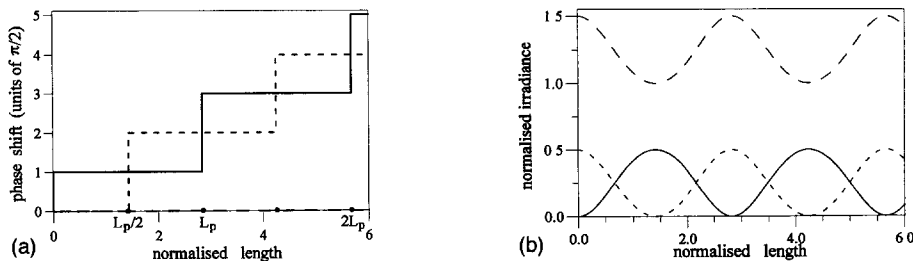


Figure 7 Typical variation in (a) the nonlinear phase shift $\phi^{NL}(z)$ and (b) fundamental and second harmonic irradiances versus normalized (to L_p) distance for Type II phase-matching for the strong fundamental I_1 (long dashed line, along horizontal axis), the weak fundamental I_2 (short dashed line) and the second harmonic (solid line). (From [61].)

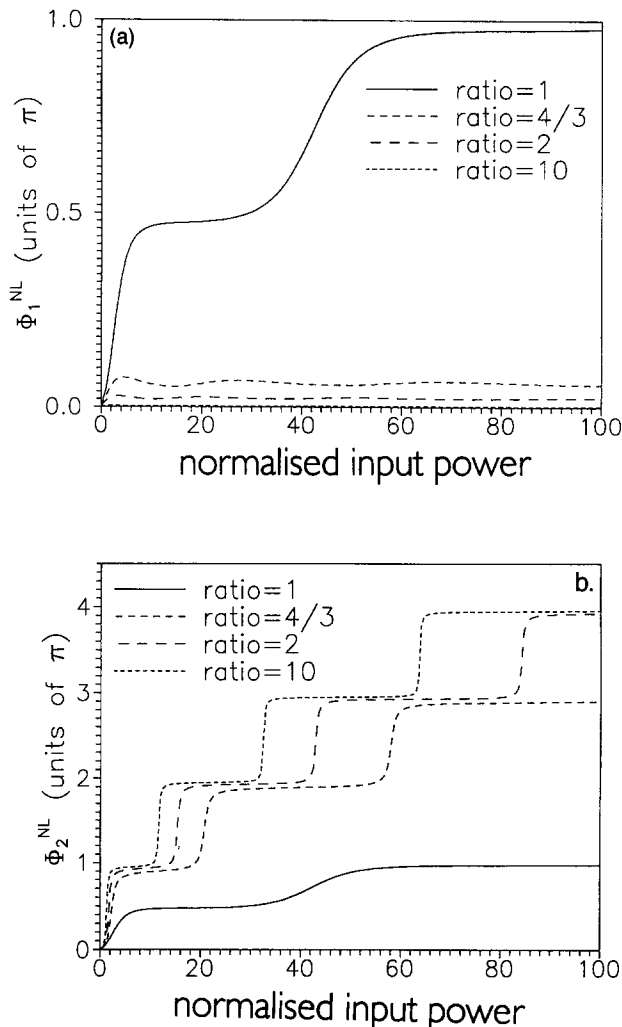


Figure 8 The nonlinear phase shift of $\phi^{NL}(L)$ of the strong (a) and weak (b) fundamental input beams versus normalized input power for various ratios of $I_1(0)/I_2(0)$ at a phase-mismatch of $\Delta kL = 0.1\pi$. (From [59].)

‘cross-phase’ modulation of the orthogonally polarized weak beam is large and the ‘self-phase’ modulation of the strong beam is small, a very unusual property for nonlinear optics. As $\delta \rightarrow 0$, the phase shift for the two fundamental beams becomes equal.

As suggested by Assanto, approaching zero imbalance between the fundamental irradiances can be very useful for all-optical transistor action [58, 59]. Consider, for example, Fig. 9 in which the fundamental throughput for the strong beam is shown. Because of the irradiance-dependence of the oscillation period with beam irradiance in the Type II case, there is a rapid oscillation in the fundamental throughput near $\delta = 0$ for small ΔkL . If the input to the crystal is biased around a region of rapid change, for example 89% in Fig. 9, and if the input is modulated about this bias point, then large gain will occur for the modulation due to the steepness of the response curve in Fig. 9. This is desirable for a power transistor.

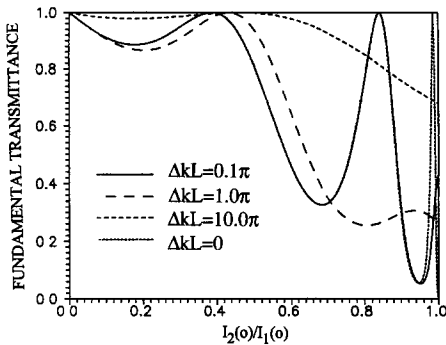


Figure 9 The throughput of the strong fundamental versus the irradiance ratio $I_2(0)/I_1(0)$ with different net phase-mismatches ΔkL . (From [58].)

Additional interesting responses can be obtained by seeding with a second harmonic at the input. Again the relative phases will play an important role and a rich variety of different outputs can be expected. Such cases have not been analysed in detail to date.

Nonlinear eigenmodes also exist for this case, as considered in detail by Kaplan [53]. The three beams must be launched with both a specific difference between the phases at the input, i.e. $\phi_3 - \phi_2 - \phi_1 = (S - 1)\pi/2$ with $S = \pm 1$, and with relative wave irradiances which are too complex to be given here (see [53] for details). These eigenmodes also have nonlinear phase shifts which are linear with distance into a medium, similar to the eigenmodes in the Type I phase-matching case.

2.1.3. Cross-phase modulation

A key question is whether the equivalent of the familiar $\chi^{(3)}$ -based cross-phase modulation is possible with cascading. Although always present with third order nonlinearities, in cascading the beams must be coupled via appropriate $\chi^{(2)}$ coefficients and there must be energy exchange between them. By default cross-phase modulation occurs between the fundamental and the harmonic, as well as between all of the waves participating in sum and difference frequency generation of which Type II SHG is a limiting case. That is, for a weak secondary input beam at a different frequency, there must be an almost phase-matched link between the strong and weak beams via sum or difference frequency mixing for there to be cross-phase modulation. This case has been considered in detail by Hutchings and coworkers [55]. The results closely resemble those already discussed for the Type II SH case.

A different form of cross-phase modulation is feasible with two orthogonally polarized fundamental inputs which are separately linked to the same second harmonic via different $\chi^{(2)}$ tensor elements. This would be difficult to implement in bulk crystals but is conceivable in waveguides. That is, a second harmonic can be generated by either one of the fundamental beams alone. This case and some of its repercussions have been considered by Assanto and coworkers [62]. There are many variables, specifically the two effective nonlinearities, detunings, relative powers, etc. Typically one of the fundamental beams is weaker than the other and it is possible to control the strong beam output just by varying the relative phase between the two inputs, i.e. the phase of the weak beam. Another operation demonstrated numerically is the large gain experienced by a weak beam over a large range of relative phases between the beams at the input. This can be potentially useful for an optical transistor or demultiplexer. The authors predicted numerically that such operations could be implemented in LiNbO₃ waveguides [62].

Introducing the extra degrees of freedom in this case also affects the stability of the system at

high powers. Trillo and Assanto have found that this cross-phase modulation scheme can lead to spatial chaos in the polarization at the output for long enough waveguides [63]. The fundamental output polarization can undergo stochastic evolution with distance so that small changes in the input power produce large polarization changes at the output.

2.2. Experimental measurements of SHG-generated nonlinear phase shifts

2.2.1. Bulk crystals

The cascaded nonlinear phase shifts have been measured directly, both in bulk crystals and in channel waveguides. The first work was by Belashenkov *et al.* in 1989 on bulk CDA [25]. Using a form of time-resolved interferometry, they were able to image the nonlinear phase change across the temporal profile of a pulse. More recently DeSalvo and coworkers using Z-scan measured the complete detuning and fundamental depletion curves near SHG phase-matching in KTP [26]. The results of that work are reproduced in Fig. 10. Note that in [26],

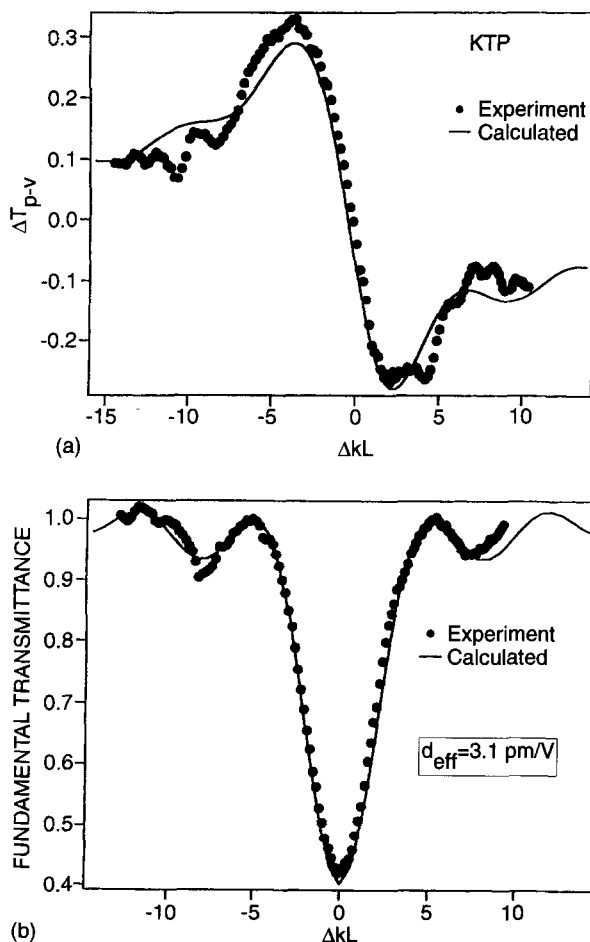


Figure 10 (a) The nonlinear phase shift $\phi^{\text{NL}}(L) [\propto \Delta T_{p-v}]$ versus detuning ΔkL for KTP measured at 1064 nm using Z-scan with an incident of 9.4 GW/cm^2 on focus. (b) The corresponding fundamental transmission. (From [26].)

the sign of the phase mismatch is defined opposite to the definition given elsewhere in this paper. The agreement with theory is excellent. What is most noteworthy is that the cascading effect at its optimum detuning was much larger than the corresponding third order nonlinearity in KTP. And this is the exciting promise of cascading, i.e. that large nonlinear phase shifts can be obtained at input irradiances much less than those currently needed for nonlinearities in the best Kerr media.

Although the non-resonant $\chi^{(2)}$ response of a material is very fast (of the order of femto-seconds), this does not mean that the linear phase shift response as shown in Figs 2–4 is also this fast. Figure 4a or 10 can be interpreted as a frequency detuning curve, showing that there is a bandwidth associated with cascading. The importance of this bandwidth depends on where the centre frequency of a pulse occurs. For large detunings, the nonlinear phase shift leads to some modification of the frequency spectrum of the pulse, i.e. $\phi^{\text{NL}}(L)$ varies with ΔkL (and therefore the $\Delta\omega$ associated with a fast pulse). The influence of the SH bandwidth becomes more severe for pulses near the phase-match condition if the pulse bandwidth is broader than the phase-matching bandwidth. This effect has been observed for β -barium borate, and the corresponding calculations are shown in Fig. 11 by Hache *et al.* [64]. These results show a significant decrease in the net nonlinear phase shift for pulses shorter than 300 fs in β -barium borate.

The nonlinear phase shift has been measured via Z-scan in KNbO_3 , CDA, KTP and β -barium borate [25, 26, 64–66]. Examples of single crystal organics which have been measured are DAN and MBA-NP [67, 68]. To date, the largest effective nonlinearities reported have been of the order of $2 \times 10^{-13} \text{ cm}^2 \text{ W}^{-1}$ obtained near phase-matching in a 0.8 mm thick DAN single crystal, a factor of five larger than CS_2 even for such a short crystal [68].

2.2.2. Waveguides

Nonlinear phase shifts in general are probably best utilized in optical waveguides in which the input power for a desired phase shift can be minimized by virtue of their strong field confinement without diffraction. The first waveguide measurements were performed by Sundheimer *et al.* using spectral broadening to deduce the phase shift in segmented, ion-exchanged KTP waveguides [69]. However the key experiments were in LiNbO_3 channel waveguides which

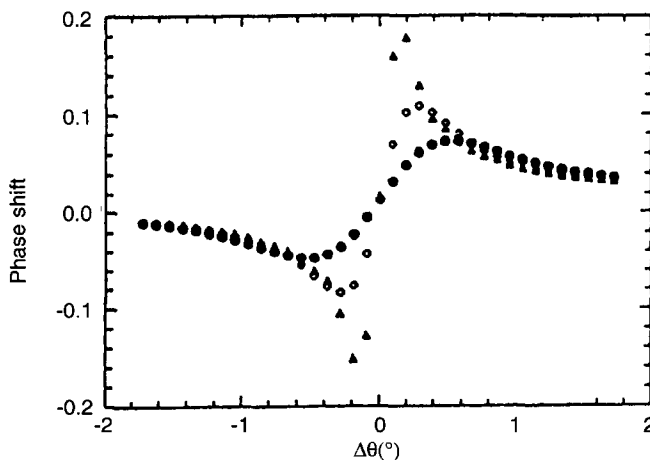


Figure 11 Calculated nonlinear phase shifts $\phi^{\text{NL}}(L)$ versus angular detuning from phase-match for 50 fs (solid circles), 100 fs (open diamonds) and 300 fs (solid triangles) pulses for constant peak input fundamental irradiance. (From [64].)

utilized temperature-tuned Type I phase-matching at 1320 nm [70]. The details of this experiment are important because of the valuable lesson learned from it. For the geometry used, the phase-matching temperature was around 340°C and an oven was necessary to operate at this temperature. Because of the short working distance of the lens required for coupling into the single mode waveguides, the sample ends were located right at the oven windows where the temperature was lower than in the central part of the oven (and waveguide). Thus, when the central part of the waveguide was wavevector-matched, the ends were not, and vice versa. This led to a highly asymmetric fundamental throughput around the temperature (336.6°C) associated with phase-matching the central part of the waveguide, as shown in Fig. 12. The nonlinear phase shift (Fig. 13) was measured directly with a Mach–Zehnder interferometer. The key point is that a large nonlinear phase shift ($> 1.5\pi$) was measured commensurate with a loss of only 10% or less to SHG at the output.

The results in Figs 12 and 13 have very important repercussions. With a uniform wavevector mismatch along the waveguide and useful nonlinear phase shifts, the throughput of the fundamental is dramatically reduced due to SHG. These LiNbO₃ results showed that this loss to SHG can be minimized with an appropriate wavevector mismatch distribution with distance. The ‘price’ for minimizing this ‘loss’ is that the required waveguide length is increased relative to the uniform wavevector mismatch case.

Cascaded phase shifts have also been measured in a single crystal core fibre using the organic DAN in the core [68, 71]. Although the fundamental mode was guided, this waveguide was below cut-off for the second harmonic which could therefore not propagate as a guided mode. The second harmonic was emitted in the form of Cerenkov radiation into the fibre glass cladding. Nevertheless, cascaded phase shifts still occurred, a fact that does not invalidate the simple model introduced above. Even in this case the harmonic exchanges energy with the fundamental within the fibre with distance. Initially the harmonic grows with distance inside the fibre core, continuously leaking energy into the cladding at each reflection from the core–cladding boundary due to the non-unity reflection at that interface. In the Cerenkov

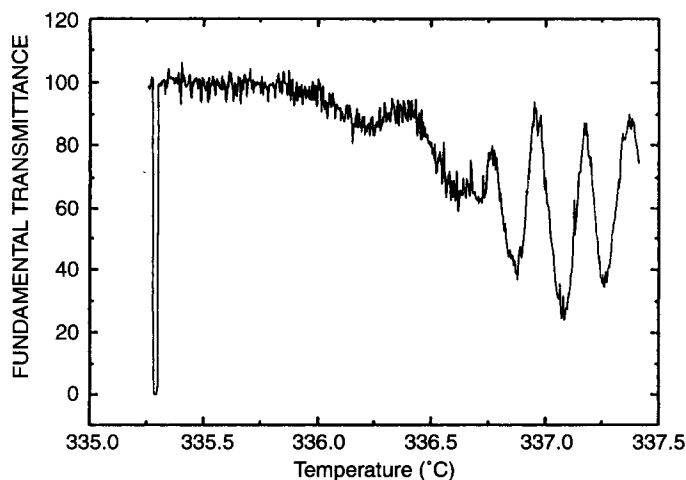


Figure 12 Fundamental transmission $P_w(L)/P_e(0)$ (in per cent) near Type I phase-matching for SHG in LiNbO₃ channel waveguides versus temperature in the centre of the oven for temperature tuned phase-matching [$(T - T_{PM}) \propto \Delta kL$]. (From [70].)

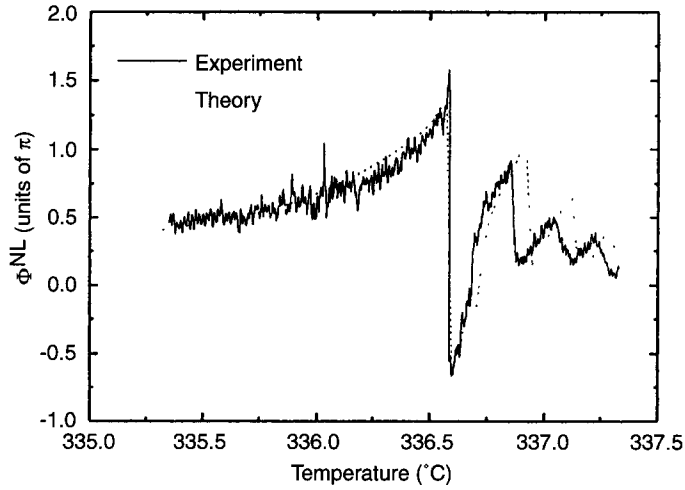


Figure 13 Nonlinear phase shift $\phi^{NL}(L)$ near Type I phase-matching for SHG in LiNbO₃ channel waveguides versus temperature in the centre of the oven for temperature tuned phase-matching. (From [70].)

SHG limit, the harmonic generated ‘between reflections’ just equals the harmonic radiated out of the waveguide, resulting in steady-state radiation into the cladding, i.e. Cerenkov SHG. Even in the steady-state region, the harmonic and fundamental trapped in the fibre continue to exchange energy and hence lead to a ϕ^{NL} . A nonlinear phase shift of $\pi/4$ was obtained with only a few tens of watts of input.

3. Effective cascaded nonlinearities via optical rectification

As mentioned in the introduction, cascaded effects can also occur due to optical rectification. Just as the second harmonic is the intermediate and necessary step for cascading using $\chi^{(2)}(2\omega; \omega, \omega)$, the optical rectification field is the intermediate step for cascading based on $\chi^{(2)}(0; \omega, -\omega)$ [10, 72]. A d.c. electric field $E_i(0)$ is created by the mixing of the fundamental field with itself via $\chi^{(2)}(0; \omega, -\omega)$

$$P_i(0) = \frac{1}{2} \epsilon_0 \chi_{ijk}^{(2)}(0; \omega, -\omega) E_j(\omega) E_k^*(\omega) = \epsilon_0 (\epsilon_{ii} - 1) E_i(0) \quad (13)$$

where ϵ_{ii} is the relative d.c. dielectric tensor component. Through a second $\chi^{(2)}$ process, essentially the electro-optic effect, and effective nonlinearity n_2^{OR} due to the optical rectification effect (versus n_2 from $\chi^{(3)}$ and n_2^{SHG} for the SHG cascading discussed previously) is obtained of the form

$$n_2^{OR} = \frac{1}{c \epsilon_0 n_1^2} \frac{[\chi_{iik}^{(2)}(-\omega; \omega, 0)]^2}{\epsilon_{kk} - 1} = \frac{n_1^6}{4c \epsilon_0 (\epsilon_{kk} - 1)} [r_{iik}]^2 \quad (14)$$

where r_{ijk} is the electro-optic tensor. The magnitude of n_2^{OR} is always positive, and depends on polarization and propagation only through the values of the second order tensor coefficients. Clearly this process again leads to an effective nonlinear refractive index change.

The contributions of n_2^{OR} to the nonlinear refraction in a Z-scan experiment have been measured by Bosshard *et al.* in KNbO₃ which has some of the biggest electro-optic coefficients

known [72]. By using the largest coefficient of 360 pm V^{-1} , an optimum n_2^{OR} of $\sim 2 \times 10^{-14} \text{ cm}^2 \text{ W}^{-1}$ was measured. For this optimum geometry they also evaluated numerically the contribution from n_2^{SHG} which was far from phase-matching and hence far from optimum, i.e. in the limit where $n_2^{\text{SHG}} \propto 1/\Delta k$. In the geometry for which n_2^{OR} is optimized, it is about one order of magnitude larger than this n_2^{SHG} . Along other directions the contributions are comparable. However, it is worth noting that near phase-matching in KNbO_3 with $d_{2,\text{eff}} = 5.6 \text{ pm V}^{-1}$, the second harmonic cascaded contribution was measured to be a factor of about four larger [66].

Recent calculations and experiments on degenerate four wave mixing have shown that the optical rectification effect is again dominant for certain polarization and propagation directions in materials with large electro-optic coefficients. This effect has been analysed by Zgonik and Günter and Unsbo [23, 73, 74]. The physical picture follows that of the usual degenerate four wave mixing process, i.e. the two counterpropagating beams (wavevectors \mathbf{k}_1 and \mathbf{k}_2) are taken with the signal input (\mathbf{k}_3) in pairs to produce two gratings (wavevectors \mathbf{k}_5 and \mathbf{k}_6) which can 'reflect' a beam into the output direction (\mathbf{k}_4). The general formalism for the optical rectification contribution to the effective third order susceptibility $\chi_{\text{eff}}^{(3)}$, leads to

$$\begin{aligned} \chi_{ijkl,\text{eff}}^{(3)}(-\omega; \omega, -\omega, \omega : -\mathbf{k}_4; \mathbf{k}_1, \mathbf{k}_2, -\mathbf{k}_3) &= \frac{3}{2} \chi_{ijkl}^{(3)}(-\omega; \omega, -\omega, \omega : -\mathbf{k}_4; \mathbf{k}_1, \mathbf{k}_2, -\mathbf{k}_3) \\ &+ \frac{\chi_{ikp}^{(2)}(0; \omega, -\omega : -\mathbf{k}_5; \mathbf{k}_1, -\mathbf{k}_3) \chi_{jlp}^{(2)}(-\omega; \omega, 0 : -\mathbf{k}_4; \mathbf{k}_2, -\mathbf{k}_5)}{\epsilon_{pp} - 1} \\ &+ \frac{\chi_{jqk}^{(2)}(0; \omega, -\omega : -\mathbf{k}_6; \mathbf{k}_2, -\mathbf{k}_3) \chi_{ilq}^{(2)}(-\omega; \omega, 0 : -\mathbf{k}_4; \mathbf{k}_1, \mathbf{k}_6)}{\epsilon_{qq} - 1} \end{aligned} \quad (15)$$

However, as pointed out by Zgonik and Günter, the physics of the material and mixing process must be taken into account in deciding which terms actually contribute. For example, in strong ferroelectrics like KNbO_3 , changes in the polarization are associated with polar optical phonons. That is, rectification terms in $\chi_{\text{eff}}^{(3)}$ which involve the generation of longitudinally polarized static fields need to be omitted.

The theory was tested experimentally in KNbO_3 and very good agreement was obtained [74]. The experiments were done with 532 nm beams so that the SHG cascading term was negligible because of the material absorption at the harmonic wavelength of 266 nm. Directions were identified which involved the largest electro-optic coefficient $r_{232} = 365 \text{ pm V}^{-1}$ and for which optical rectification dominated the relevant $\chi^{(3)}$ component by a factor of 15–20.

3.1. All-optical switching devices

3.1.1. Waveguide devices

There has been a concentrated effort in the last 10 years to implement all-optical switches in waveguides which operate with reasonable peak powers [27, 75]. Their purpose is to direct the input signal either to one of two possible outputs (nonlinear directional coupler, NLDC), or to modulate it (nonlinear Mach–Zehnder interferometer, NMZI), both depending on the irradiance of either the signal itself, or that of a control beam. These devices require a nonlinear phase shift of 2π and π respectively and have already been successfully implemented with a variety of third order nonlinear mechanisms [75]. Assanto *et al.*, Schiek and others have shown theoretically that the cascaded nonlinear phase shifts can indeed be used for all-optical switching devices [43, 48, 76–78]. In fact, Schiek has given a very complete analysis of

all-optical switching with an NLDC, including switching with temporal solitons supported by the cascading nonlinearity [43, 76].

Picciau and colleagues have extended the cascading nonlinearity to Bragg periodic structures [79]. The system is complicated by the presence of four waves inside the structure, a fundamental and harmonic travelling in both directions. Amongst the rich variety of all-optical response was a versatile bistable gate, and many features different from those expected from classical Kerr nonlinearities.

Both an NMZI and an NLDC have been demonstrated in LiNbO₃ channel waveguides in which the cascaded nonlinear phase shift is used to mimic a third order nonlinearity [80–82]. The waveguides used were similar to those described in section 2.2. That is, the wavevector mismatch varied with position in such a way that the net conversion at the output to SHG was only of order 10% and the nonlinear phase shifts were large, $> 2\pi$. The design needed was quite sophisticated, especially for the NLDC (inset of Fig. 14) because there are four fields involved, and there is potential coupling between the two fundamentals and between the two second harmonics in the two parallel waveguide arms [82]. The output from the two channels as a function of input power is shown in Fig. 14. Note that the response does not show any large oscillatory behaviour superimposed on the switching curves. Such oscillations are expected from an NLDC with uniform wavevector mismatch [43, 48, 76]. However, the switching power is currently larger than the best $\chi^{(3)}$ -based and active semiconductor amplifier devices [75]. This is primarily because the nonlinearity for this cut of LiNbO₃ (5 pm V^{-1}) is small.

An NMZI has also been successfully implemented by the same authors, both in hybrid and completely integrated formats in LiNbO₃ channel waveguides [80, 81]. The hybrid device interfered a cascaded phase shift in an LiNbO₃ channel waveguide with a reference beam propagated in a linear medium. For the fully integrated version, different channel widths were fabricated to produce different wavevectors. This resulted in different wavevector mismatches in each channel and hence different nonlinear phase shifts. The switching

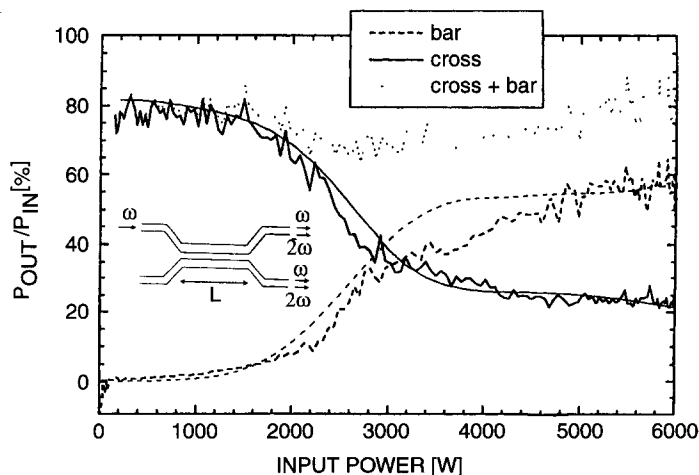


Figure 14 The all-optical response of a nonlinear directional coupler based on cascading nonlinearities in LiNbO₃ channel waveguides using temperature tuned Type I phase-matching. The geometry is shown in the inset. The percentage of fundamental power $P_{\omega}(L)/P_{\omega}(0)$ outputted from the bar (incidence) and cross (neighbouring) channels is plotted versus input fundamental power. (From [82].)

characteristics were excellent, even though pulses were used. Although these devices also required relatively large powers for switching, just like the NLDC, the key point is that they can be implemented based on the cascading nonlinearity.

3.1.2. Intracavity SHG devices

Optical bistability initiated the interest in all-optical devices over 20 years ago and has been implemented with just about every known nonlinear mechanism which changes the refractive index [83]. The effects of cascading on SHG in cavities has led to interesting effects, including optical bistability [84–86]. In some cases the origin of the bistability is not attributed to cascading nonlinearities although they seem to be a reasonable candidate for the response observed [84]. The role of cascading has been recognized in a number of cases. For example, by placing KNbO_3 in an optical cavity and implementing Type I phase-matching of a Ti:sapphire laser, Ou has observed asymmetries in both the fundamental and harmonic temporal line shapes [85]. Although the details of the experiment have not yet been explained, it is clear that the cascading process in some form is responsible for the observations because the effects depend on the detuning from phase-match [85]. With his available theory, Ou deduced a huge cascading phase shift of 5π .

In a very recent report, White and coworkers clearly observed and interpreted cascaded bistability in a monolithic LiNbO_3 resonator tuned for SHG with 1064 nm input [86]. The wavevector mismatch was adjusted by temperature tuning and the laser frequency was then swept through the resonance and the line shape function measured. A nonlinear phase shift is accumulated in the cavity away from the phase-matching condition, which acts to pull the cavity back towards resonance during the strong illumination part of the cycle. The result is shown in Fig. 15. There are three important features: (1) bistability occurs when the linear and nonlinear detunings are of opposite sign; (2) the line shape at powers above a 125 mW threshold is asymmetric and exhibits bistability; and (3) the direction of both the bistable loop and the line asymmetry reverses when the process is tuned to opposite sides of phase-matching. Most remarkable here are the low powers required for bistability, and the high quality of the bistable response. Note that the SHG losses had to be minimized by operating near the first zeros of the SHG response curves. This allowed the cavity to have a high enough finesse to make the bistability occur at such low powers. The agreement with theory was very good.

Reinisch and colleagues have analysed the problem of coupling into $\chi^{(2)}$ -active waveguide resonators near their phase-matching conditions for both resonant excitation of the guided modes and for SHG [87, 88]. They used the usual coupled mode equations for prism or grating coupling, augmented by the SHG interaction (Type I). Under steady state conditions, i.e. infinite plane wave illumination approximation, they found that the cascaded phase shifts should lead

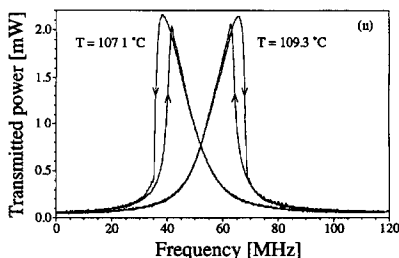


Figure 15 Optical bistability in an LiNbO_3 resonator temperature detuned on both sides of phase-matching versus frequency tuning of the incident laser. (From [86].)

to optical bistability with appropriate detuning and irradiance thresholds [87]. However, when the input was seeded with a second harmonic, bistability was predicted above a threshold power for the seed and over a range of different phase angles between the two inputs, even on phase-matching [88]. They linked this bistability to a nonlinear resonance of the waveguide coupler-seeded SHG interaction. In the absence of a fundamental input, this resonance also leads to parametric down-conversion of the incident harmonic into the fundamental once the parametric instability threshold is crossed.

3.2. SHG mode competition in waveguides

Second harmonic generation has been investigated in channel waveguides for over 20 years and has reached a high level of sophistication [31, 89]. Quite frequently waveguides which are single mode at the fundamental wavelength are multimode at the harmonic. Therefore, as the input wavelength is scanned, phase-matching to harmonics corresponding to different waveguide modes occurs at different wavelengths. Because the harmonic modes are separated from one another by at least a few SHG bandwidths, their SHG responses are expected to be independent of each other.

However, looking at Fig. 4a, we see that the nonlinear phase shift can still be quite large, many linewidths away from an SHG resonance if the input power is high enough or the nonlinear coupling coefficient (κ) is sufficiently large [90]. If only one fundamental mode is excited and if two harmonic phase-matching resonances (two different modes) are possible, then the two harmonics are both excited to some degree and hence they compete with each other for the fundamental power. Furthermore, a nonlinear phase shift due to each harmonic resonance is induced at every wavelength, even at the centre wavelength for SHG of the other mode. This nonlinear phase shift varies with distance into the waveguide as shown in Fig. 2a. It is further complicated due to the mode competition for power which also varies along the waveguide. The net result is that the phase-matching condition which includes the nonlinear component will vary with distance from the input. This implies that the wavelength of maximum conversion can change its centre wavelength and the normalized figure of merit for SHG will depend on fundamental input power and waveguide length.

Such effects have been observed experimentally in quasi-phase-matched LiNbO₃ waveguides with fundamental wavelengths in the 1500 to 1600 nm range [90]. Examples of the SHG detuning curves are shown in Fig. 16 along with pictures of the actual mode patterns seen at different wavelengths. Note the changes in the peak positions with increasing incident power as evidenced by the arrows, and the changes in the relative conversion efficiencies.

3.3. Degenerate and almost degenerate four wave mixing

A number of experiments have been reported in which two successive $\chi^{(2)}$ processes have been used to mimic four wave mixing. In the cascading context, first a second harmonic beam is generated by one of the input beams, and then difference frequency mixing between that SH beam and the second input beam leads to the signal of interest. Back in the 1980s Baranova and Zeldovitch analysed this case and predicted that large cross-sections should be achievable [15].

Two particular variations of this process have been demonstrated [64, 66, 91, 92]. In the first, two equifrequency (ω) beams with wavevectors \mathbf{k}_1 and \mathbf{k}_2 are incident in slightly different directions near the phase-matching condition and overlap inside the sample. When wave 1 is doubled (2ω) and wave 2 mixes with this harmonic via difference frequency generation, a new beam (at $2\omega - \omega \rightarrow \omega$) near the phase-matching condition with wavevector $2\mathbf{k}_1 - \mathbf{k}_2$ is

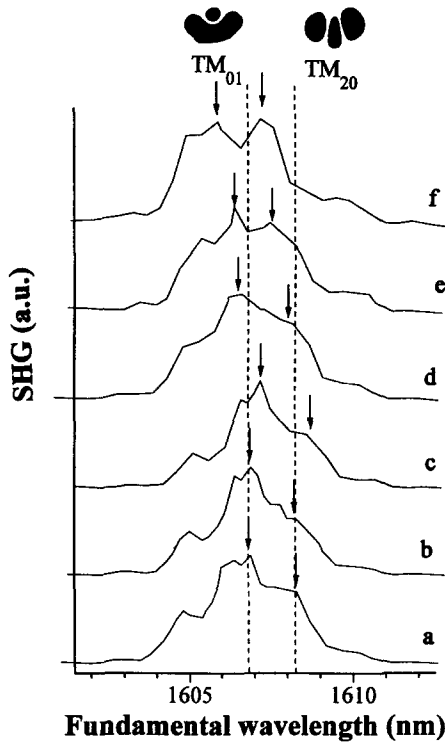


Figure 16 Variation in the second harmonic detuning curves for two closely spaced (in wavelength of the fundamental) second harmonic modes in a multi-mode LiNbO₃ channel waveguide at different input powers. The maximum conversion efficiencies $\eta = P_{2\omega}(L)/P_{\omega}(0)$ and the input fundamental powers P_{in} (η, P_{in}) are: (a) (0.005%, 4 mW); (b) (0.069%, 15 mW); (c) (0.63%, 60 mW); (d) (17%, 38 W); (e) (23%, 103 W); and (f) (27%, 113 W) respectively. The positions of the peak second harmonic powers (arrows) and the guided wave modal profiles are also shown. (From [90].)

generated. Of course the complementary output at $2k_2 - k_1$ is also generated via harmonic generation of wave 2. If these two new beams are strong enough, they generate another pair of beams via cascading, and so on. The generation of a sequence of such beams was demonstrated by Danelius and coworkers in β -barium borate with 1064 nm inputs [91]. The results shown in Fig. 17 indicate the generation of at least six extra beams.

This particular interaction has an interesting application to the control of the frequency chirp

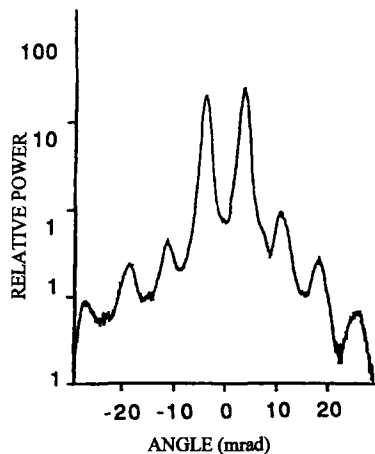


Figure 17 The relative output beam powers (all at the frequency ω) observed versus angle away from the phase-matching angle due to multiple, successive four wave mixing processes via cascading. The two strongest peaks correspond to the unconverted input beams. (From [91].)

of pulses [92]. For example, if wave 1 has a frequency chirp α_1 and wave 2 a chirp α_2 , then the frequency chirp of the beam scattered into the direction defined by $2\mathbf{k}_1 - \mathbf{k}_2$ is $2\alpha_1 - \alpha_2$. This becomes especially interesting if $\alpha_2 = -\alpha_1$ so that the frequency chirp in the new beam is $3\alpha_1$, which can subsequently be used for enhancing pulse compression. In the experimental verification, a tripling of the frequency chirp was indeed observed and used for pulse compression. Because a cascaded nonlinear phase shift occurs on the down-conversion step back to the original fundamental beam (wave 1 in this case), it is not present in the scattered beam resulting in a clean transfer of the chirp.

The second case has potential applications to frequency shifting in communications. This requires two collinear input beams, one at ω (strong beam) and the other at $\omega - \Delta\omega$ (weak beam). The process is arranged to be near phase-matching for doubling the strong beam. Then difference frequency generation occurs via mixing of the weak beam and the harmonic which leads to a beam at $\omega + \Delta\omega$, that is the frequency has been shifted by $2\Delta\omega$. Equivalently a signal at $\omega + \Delta\omega$ can be shifted by $-2\Delta\omega$.

The efficiency of this process has been demonstrated in MBA-NP and β -barium borate crystals at 1064 nm [64, 66]. Results for MBA-NP are reproduced in Fig. 18. Although the $d_{\text{eff}}^{(2)}$ was only 2.5 pm V^{-1} , the conversion efficiency $\xi = [W_{\omega+\Delta\omega}/W_{\omega}^2 W_{\omega-\Delta\omega}] n^4/L^2 \propto |d_{\text{eff}}^{(2)}|^4$ was impressive for 100 MW cm^{-2} pump irradiances where W is the pulse energy. For calibration, the signal obtained via $\chi^{(3)}$ from BK7 glass is shown, as well as for two different field polarization directions in which the MBA-NP crystal is far from phase-matching.

3.4. Gain and transistor action via cascading

A number of characteristics of the cascading process discussed in the theory section suggest that it could be used as an optical transistor. To date, several schemes for applying cascading in second-harmonic generating (SHG) crystals to optical transistor-like devices have already been proposed and demonstrated [48–52, 57–62, 93–97]. Such devices allow a weak signal beam to impose a large amplitude modulation on a strong ‘pump’ beam, through wave mixing in a $\chi^{(2)}$ crystal, or vice versa. Owing to the coherent nature of the cascaded nonlinearity, there are two distinct classes of cascading used to obtain transistor-like action, phase and amplitude controlled modulation. Numerical studies show that if a weak SH beam is input, both the amplitude and phase of the fundamental output can be controlled with the phase and/or amplitude of this seed, leading to new applications to switching devices including small-signal gain and transistor action [48, 49, 51, 52]. Another example is to use Type II SHG in which the relative

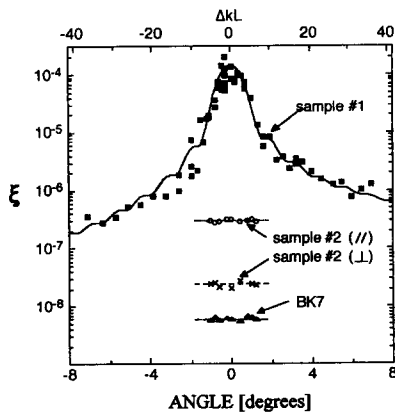


Figure 18 The conversion efficiency $\xi = [W_{\omega+\Delta\omega}/[W_{\omega}^2 W_{\omega-\Delta\omega}] n^4/L^2$ for frequency shifting an input beam (at ω , 1064 nm) to $\omega + \Delta\omega$ via cascading in MBA-NP versus angle detuned from phase-matching (ΔkL) of the strong fundamental beam. Here W is the pulse energy. To show the large cascading enhancement, the signals obtained far away from phase-matching in MBA-NP and from a reference sample of BK7 glass are also shown. (From [65].)

amplitudes of the two input fundamental beams are used to control the output [57–62]. This second case utilizes the rapid change in the fundamental throughput and SHG efficiency as the fundamental irradiances approach equality, see section 2.1.2.

We first discuss the phase controlled process through second harmonic seeding which does not have an analog with $\chi^{(3)}$ nonlinearities. The idea was discussed previously in section 2.1.1.2. The key is Fig. 6 which shows the response of the fundamental throughput as a function of relative phase angle between the seed and fundamental. To our knowledge only one experiment has been performed and this involves SHG in KTP with a weak SH seed beam [48]. A 4.6 to 1 switching ratio was achieved for a 1064 nm fundamental by modulating the relative input phase of the 530 nm control beam having 3.4% of the fundamental peak irradiance (or 18% of the peak field as it is the field that is of consequence). Figure 19 shows the fluence transmittance (i.e. on axis) of a 1 mm thick KTP crystal with $\Delta kL = 1.3$ as a function of the phase difference, $\Delta\phi = \phi_3 - 2\phi_1$ at a fixed fundamental input irradiance of 20 GW cm^{-2} . Temporal averaging over the 40 ps (FWHM) of the pulses gives the observed modulation ratio of 4.6 to 1 which agrees with the numerical calculation shown by the solid line. This modulation scheme requires that the seed beam which can be used to control the strong fundamental beam (pump) must be coherent with the pump. This is also true even if the seed modulates the pump through amplitude modulation, which is equally possible.

Although the phase sensitivity of the cascaded interaction may be exploited in some circumstances, it may be impractical because it requires interferometric stability between input beams and consequently between successive switching devices. A device of this nature is also very limited in application, as the pump and signal must be derived from the same source. This phase-sensitivity problem may be avoided by the use of Type II second-harmonic interactions where orthogonally polarized fundamental beams produce SHG even when mutually incoherent. Two groups have successfully pursued this concept [58, 93–97]. The approach is based on a feature of Type II SHG discussed previously in section 2.1.2, most specifically Equation 12 which predicts that the fundamental throughput oscillates with propagation distance and the relative irradiance of the two inputs I_1 and I_2 . As $I_1 \rightarrow I_2$, the oscillation period $\rightarrow \infty$ and the fundamental throughput can go from maximum to minimum (which corresponds to maximum SHG).

Assanto and coworkers have measured a large increase in the fundamental transmission on phase-matching when the input angle was rotated away from 45° giving $I_1 \neq I_2$ [93, 94]. Their results for fundamental transmission as a function of irradiance imbalance are reproduced in Fig. 20 for a 2 mm KTP crystal excited at 1064 nm [94]. When the results are averaged over

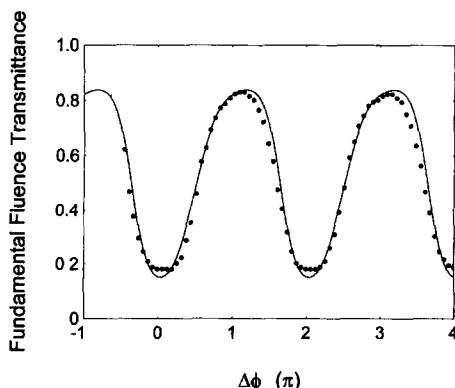


Figure 19 The fundamental throughput on phase-matching for a weak second harmonic seed (3.4% energy of the fundamental) versus relative phase angle $\Delta\phi = \phi_3 - 2\phi_1$ at the input. 1064 nm pulses were used and KTP was the doubling crystal. (From [49].)

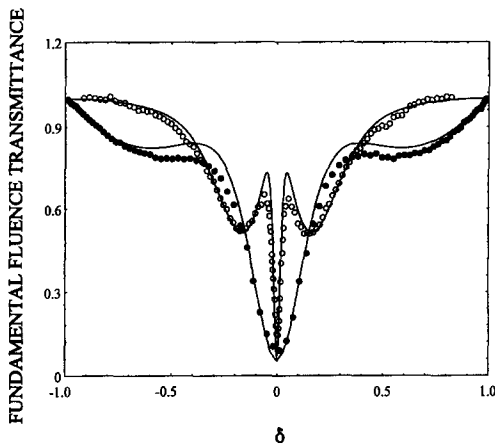


Figure 20 The fundamental (1064 nm) throughput versus the relative difference in the incident irradiances, δ , of the two orthogonally polarized fundamental beams at two different input irradiances. The solid lines are the theoretical fit. Open circles: $I_{in} = 12 \text{ GW cm}^{-2}$. Solid circles: $I_{in} = 6.2 \text{ GW cm}^{-2}$. (From [94].)

the temporal profile of the pulse, excellent agreement with theory was obtained. Considering the fundamental polarized at 45° as the pump beam, a small additional signal which creates an irradiance imbalance in one of the inputs is amplified as the net output increases dramatically. Such a gain has been measured in an independent experiment by LeFort and Barthelemy who added a polarizer at the output to block the fundamental output for the pump beam when $I_1 = I_2$ [95]. The factor of 70 gain obtained by using pump energies of $200 \mu\text{J}$ in 35 ps pulses is shown in Fig. 21. Subsequently they extended their experiment by measuring the transmittance as a function of the irradiance imbalance between the inputs [96].

Wang *et al.* have proposed a novel optical transistor which is insensitive to the relative phase between input beams by using two Type II SHG crystals in tandem [94, 97]. The first crystal couples the mutually incoherent signal to a strong 'pump' wave, while the second crystal amplifies the coupled modulation. The configuration is shown schematically in Fig. 22. The pump beam is split into two, approximately equal, orthogonally polarized components. One of these, I_1 , passes through the first nonlinear crystal (the 'coupler'), where it is modulated by the weak, incoherent signal I_s with a gain of less than unity. The key feature of the device is the method of imposing a modulation on I_1 from a weak signal, I_s , that can be temporally incoherent with both fundamental pumps. This modulated pump is recombined with the other component of the pump and incident on the second crystal (the 'amplifier'), where the modulation is strongly amplified. This is seen in Fig. 23, where the output fundamental irradiance is plotted as a function of input for different biases, where the bias is defined by

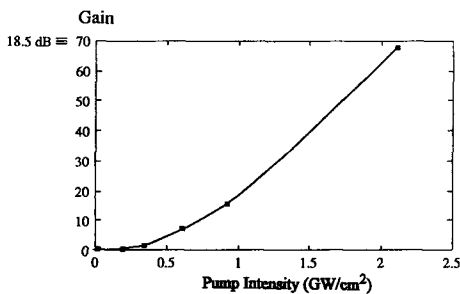


Figure 21 The all-optical transistor gain for a $1 \mu\text{J}$ input signal pulse from a KTP crystal versus fundamental input pump energy for 35 ps pulses at 1064 nm. (From [95].)

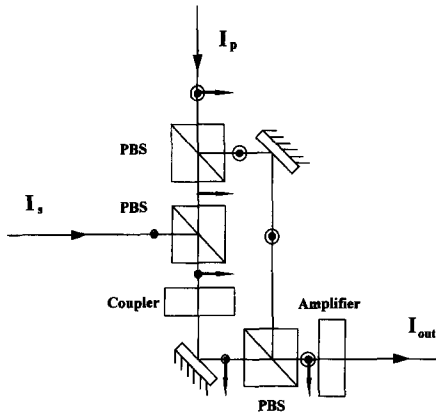


Figure 22 Schematic of a phase-insensitive all-optical transistor based on two successive Type II SHG processes. (From [94].)

$\delta = (I_1 - I_2)/I_1$. For small δ , the modulation of the transmitted irradiance is directly proportional to δ . An amplifier of this type is fundamentally different from a laser amplifier in that it has no amplified spontaneous emission. The gain also may have a narrow bandwidth and has the potential to be rapidly switched by control of the pump waves. In principle a polarizer can be added at the end of the device to block all light unless the signal is present to eliminate a background signal, but this becomes an interferometric device with the incipient dependence on the relative phase between pump waves.

3.5. Mode-locking of lasers

The application of second order nonlinearities to the mode-locking of lasers was developed quite independently from the other cascading effects described in this review. Despite this, the similarities between the ideas generated in the two fields are remarkable, as we shall demonstrate. Techniques using cascading to mode-lock lasers have seen steady improvement, from the initial studies in 1988 [32, 98] that were only applicable to high peak power pulsed systems, to the current state-of-the-art, where cw mode-locked and diode pumped systems have been demonstrated [33, 99, 100]. Most of the work in this field has its roots in the original papers of Stankov in 1988 [32, 98], where a ‘nonlinear mirror’, made from an SHG crystal and a dichroic mirror, was used as a positive-feedback, amplitude-modulation intracavity element to provide passive mode-locking and Q-switching. The first demonstration of such mode-locking was presented by Stankov and Jethwa [32], where a nonlinear mirror was used to mode-lock

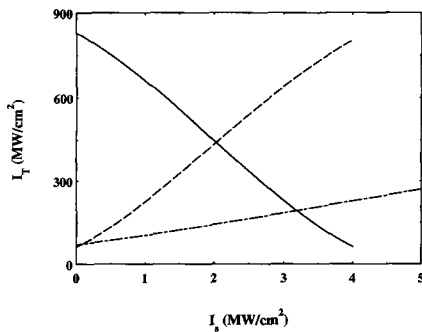


Figure 23 Calculated transistor output versus input signal for a 1 cm KTP amplifier. $I_T = 1.0 \text{ GW cm}^{-2}$, bias = 1 MW cm^{-2} (dashed line); $I_T = 1.0 \text{ GW cm}^{-2}$, bias = -5 MW cm^{-2} (solid line); $I_T = 0.6 \text{ GW cm}^{-2}$, bias = 4 MW cm^{-2} (long-short dashed line). (From [94].)

an Nd:YAG laser, producing 100 ps pulsewidths in a 100 ns train of about 3 mJ total energy. This paper also presented a simple theory for the nonlinear mirror, elaborated on by Stankov in [98], that we will describe below. It is noteworthy that this analysis, and most of the many ensuing papers on the subject, assumes only phase-matched interactions, ignoring the phase-mismatched case. It was not until much later, after significant growth of the field of cascaded nonlinearities, that the value of phase-mismatched interactions was recognized.

The nonlinear mirror in question, hereafter referred to as the ‘Stankov Mirror’, is shown in Fig. 24. Light at the laser emission frequency, ω , is incident on the phase-matched SHG crystal, sufficient to provide substantial conversion to the second harmonic under mode-locked operation. The dichroic mirror reflects 100% of the light at 2ω ($R_{2\omega} = 1$) while only partially reflecting the fundamental $R_{\omega} < 1$. Upon re-entering the SHG crystal on the return path, the interaction between the ω and 2ω waves will depend on their relative phase, $\Delta\phi$. This is similar to the behavior of the Type I, seeded SHG, described in section 2.1.1.2. For $\Delta\phi = -\pi/2 + 2m\pi$, where m is an integer, further conversion to the second harmonic will take place, but for $\Delta\phi = +\pi/2 + 2m\pi$, the energy will convert back to the fundamental. Note that the sign of $\pi/2$ may vary in the literature because of different notations. The latter case gives the condition under which positive feedback will take place, the higher the incident irradiance, the greater is the energy at the second harmonic incident on the dichroic mirror and hence the higher is the reflectance of the overall device. The device essentially provides mode-locking by mimicking the behaviour of a saturable absorber, but is different in two advantageous ways: (1) it is based on a reversible process that has the potential to be lossless; (2) the mechanism is instantaneous so the pulse shortening is equally effective on both rising and trailing edges of the pulse. However, the minimum pulsewidth is limited by the bandwidth of the SHG process, which is dictated by phase-matching considerations. Adjustment of $\Delta\phi$ proves to be relatively simple in practice, as dispersion in air may provide the necessary phase shift, with adjustment being achieved by variation of the distance from the SHG crystal to the mirror. An alternative scheme uses the tilting of a glass plate to provide a more convenient method to adjust $\Delta\phi$. The operation of the Stankov Mirror is best illustrated by Fig. 25, taken from [98], which shows the propagation of the irradiances at ω and 2ω as they propagate through the SHG crystal on their initial and return paths for $\Delta\phi = +\pi/2 + 2m\pi$ and $R_{\omega} \ll 1$. Here, the similarity to the operation of the SH-seeded optical transistor described in section 3.4 is clear.

Under the condition of $\Delta\phi = +\pi/2 + 2m\pi$, the irradiance-dependent reflectance is given by [98],

$$R(\eta) = G\{1 - \tanh^2[\sqrt{G} \tanh^{-1}(\sqrt{\eta}) - \tanh^{-1}(\sqrt{\eta/G})]\} \quad (16)$$

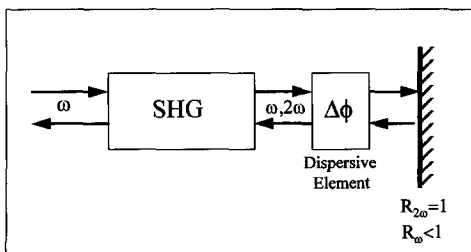


Figure 24 Schematic of the nonlinear mirror based on SHG. $R_{2\omega}$ and R_{ω} are the reflectances at the SH and fundamental wavelengths, respectively.

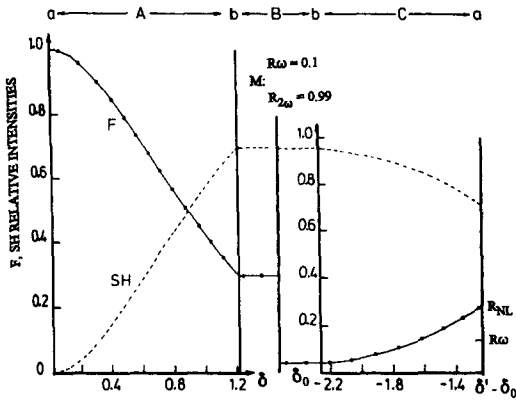


Figure 25 Dependence of fundamental and SH irradiances as they propagate through the SHG crystal on their initial and return paths, for a dichroic mirror with 100% reflectance at the SH and 1% at the fundamental, with $\Delta\phi = +\pi/2 + 2m\pi$. (From [98].)

where $G = \eta + (1 - \eta)R_\omega$, η is the conversion efficiency to second harmonic after the first pass through the SHG crystal and it is assumed that $R_{2\omega} = 1$. This behaviour is plotted in Fig. 26 for various values of R_ω . Clearly, making R_ω smaller causes the nonlinearity of the mirror to be more pronounced, as is appropriate for Q-switched operation. We will see later that relatively large values of R_ω are appropriate for cw mode-locking.

This positive feedback, amplitude-modulator form of the Stankov Mirror was the subject of many experimental and theoretical studies over the next few years. In 1989, Stankov refined the mode-locking of an Nd:YAG laser to produce transform-limited, 45 ps pulses [101], later producing even shorter pulsewidths by using a BBO crystal [102]. Mode-locking of an Er:YAlO₃ laser at 1660 nm and an Nd:YAlO₃ laser at several wavelengths was also demonstrated [103–105]. Theoretical studies of mode-locking by this technique were presented by several authors [106–110]. The problem of group-velocity mismatch (GVM) in the SHG crystal, was described by Stankov *et al.* in 1991 [111]. The same authors proposed a scheme to compensate for GVM, where a birefringent plate is placed between the nonlinear crystal

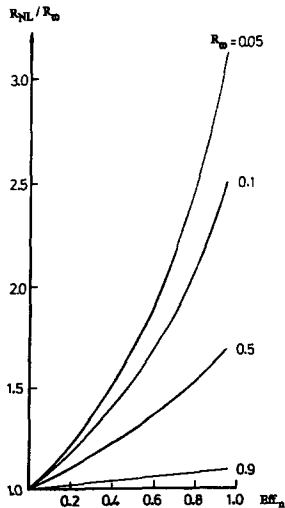


Figure 26 Overall reflectance at the fundamental for the Stankov mirror as a function of single-pass conversion efficiency, η , for several values of R_ω . (After [98].)

and the dichroic mirror [112]. However, their analysis indicates that GVM should become a problem only for pulsewidths close to or less than 1 ps, and they did not experimentally demonstrate GVM compensation. However, GVM was studied in more detail in 1995 by Xue and Lou [113] who indicated that the effects of GVM may be more severe than estimated in [111] and [112]. Experimentally, the birefringent plate compensation was first demonstrated in 1995 by Cerullo *et al.* [114], who showed that the technique could significantly shorten the pulsewidth of Nd:YAG and Nd:YLF lasers, as we will describe below.

A slight modification of the Stankov Mirror to produce mode-locking by negative feedback was first introduced in 1991 [115]. It was previously shown that the introduction of a negative-feedback element (i.e. one that has loss that increases with irradiance) to a cavity mode-locked with a positive feedback element can produce superior performance [116]. It is straightforward to achieve negative feedback with an intracavity SHG element such as the Stankov Mirror. All that is required is to make $\Delta\phi = -\pi/2 + 2m\pi$. Using this technique, long pulse trains are produced in an Nd:YAG laser mode-locked by an active acousto-optic mode-locker and a nonlinear mirror using BBO [115]. This performance was later improved upon by use of an LiIO_3 crystal in the negative feedback configuration in an actively mode-locked Nd:YAG laser cavity to produce stable pulse trains in excess of 1 ms, limited only by the flashlamp pulsewidth [117]. In the absence of the negative feedback, 600 ns bursts of mode-locked pulses at fluctuating intervals of 5–10 μs are produced.

Another variation of the Stankov Mirror was introduced by Barr and Hughes in 1989 and uses a coupled cavity configuration [118]. Here, 30–50 ps pulses are produced in a Q-switched, mode-locked train from an Nd:YAG laser. Subsequent theoretical analysis by the same authors [119] models the mode-locking as an amplitude modulation effect, but shows it can occur via either positive or negative feedback. It was noted, however, that by choosing different values of $\Delta\phi$, pure phase modulation is possible, though this was not explored.

It is interesting to note at this point that all of the cases mentioned so far consider the case of perfect phase-matching. This does not necessarily preclude the possibility of phase modulation, however, as hinted at in [119] above. As seen in section 2.1.1.2, if $\Delta\phi \neq \pm\pi/2$, nonlinear phase shifts may occur, even for $\Delta kL = 0$. Although the analysis for the systems described so far assume pure amplitude modulation, the experiments were performed on pulsed-flashlamp pumped lasers, where the dynamics of Q-switching and mode-locking are complicated. Given that it is difficult to know $\Delta\phi$ with any degree of certainty in these systems, it is probable that nonlinear phase shifts associated with the cascading may have played a role in some of them. That this was not considered in the early models for mode-locking with the Stankov Mirror, may be attributed to the independence of the respective fields of mode-locking and of cascaded nonlinearities.

The first serious consideration of nonlinear phase shifts through cascading as applied to mode-locking was by Zhao and McGraw in 1992 [120], who provided a detailed analysis of a phase-matched ‘parametric mirror’, which is a nondegenerate frequency mixing variation of the Stankov Mirror. Such a device was originally proposed in 1988 by McGraw [121] with a similar concept presented in 1989 by Stankov [122]. Stankov proposed using such a device synchronously to mode-lock two lasers running at different wavelengths, although this has not been realized experimentally. Zhao and McGraw used their device to provide AM mode-locking in a sync-pumped dye laser, although the process reported requires an external laser pulse to participate in the nonlinear mixing process. The effect of the parametric mirror is to reduce the pulsewidth from 13.7 ps in the pure sync-pumped case to 7.5 ps with the parametric mirror. This is probably the first case of cw mode-locking using a second order

nonlinearity, albeit a hybrid mode-locking system. Although, in their analysis, the authors made no connection to the work in cascaded nonlinearities, they clearly showed how nonlinear phase shifts could be produced in the case of $\Delta kL = 0$. The use of this effect for FM mode-locking was proposed and analysed, but was not experimentally realized. In retrospect, the difficulty of applying nonlinear phase shifts to the mode-locking of such a cavity may be the strong self-focusing or defocusing that results from such nonlinear phase shifts [26].

There are some cases where cascaded nonlinear phase shifts have clearly played a role in mode-locking, although the authors may not have been aware of the exact mechanism at the time. In 1990, Carruthers and Duling [123] used a KTP crystal, cut for Type II SHG, in an anti-resonant ring to mode-lock an Nd:YAG laser as shown in Fig. 27. Under cw flashlamp pumping, self-starting mode-locking with 11 ps pulses was observed when Faraday rotators were oriented to make the counter-propagating beams cross-polarized. The mode-locking was particularly sensitive to alignment of the KTP crystal and it was noted that optimum mode-locking could be found with a slight phase-mismatch, indicating that nonlinear phase shifting could be a possible mechanism for the mode-locking. Indeed, the authors did attribute the mechanism to phase modulation, but it was left to DeSalvo *et al.* [26] to point out the possible connection between this experiment and cascaded nonlinear phase shifts. In 1993 Wu *et al.* [124] also observed mode-locking in a cw Nd:YAG laser with an intracavity KTP SHG element. In this case, the mode-locking had to be forced by moving one of the end mirrors, but similar to reference [123], optimum mode-locking was observed with a slight phase-mismatch. Again, self-phase modulation in the KTP is given as the mode-locking mechanism but this was attributed to $\chi^{(3)}$ rather than $\chi^{(2)}$.

Probably the first clear demonstration of passive cw mode-locking using the positive feedback Stankov Mirror was in 1994 by Danailov *et al.* in Milan [99]. There, a cw flashlamp pumped Nd:YLF laser was mode-locked with an intracavity LBO SHG crystal. To facilitate self-starting mode-locking, the dichroic mirror had a relatively high fundamental reflectance of 77.5%, and the cavity was designed to produce a small mode area in the SHG crystal, with a much larger mode size in the laser rod. The laser produced near transform-limited pulses of 13 ps duration at a wavelength of 1047 nm with an average power of 1.5 W. The same year, the Milan group demonstrated the first mode-locking of this type in a diode-pumped laser [100]. In this case, an Nd:YAG laser, pumped with 3.2 W of power from two GaAlAs diode lasers, was mode-locked using a temperature tuned LBO crystal in a geometry similar to that of [99]. Pulses of 10 ps duration were produced in a beam of 700 mW average power. Figure 28 shows

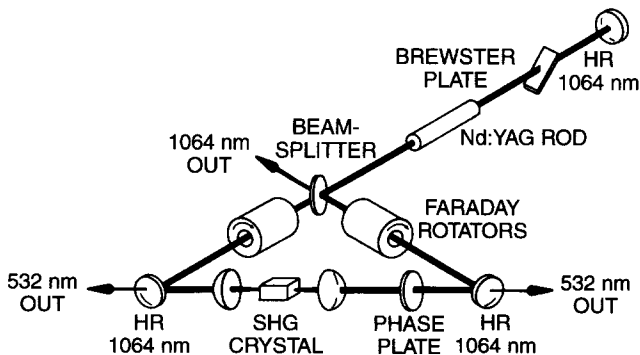


Figure 27 Schematic of cw mode-locked laser using KTP as the passive mode-locking element in an anti-resonant ring. (From [123].)

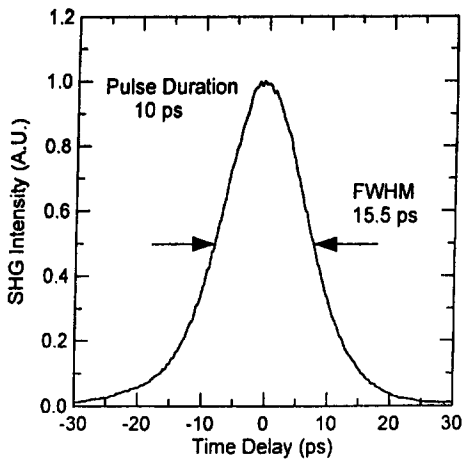


Figure 28 Autocorrelation of mode-locked output from the diode-pumped Nd:YAG laser [100]. The laser is mode-locked with an LBO SHG crystal.

an autocorrelation trace used to determine the pulsewidth. The analysis in this paper is of particular interest as it clearly describes the near equivalence of changing the relative phase, $\Delta\phi$, and changing the phase-mismatch, ΔkL , although the application to nonlinear phase modulation is not mentioned.

It was not until 1995 that the theory of nonlinear phase shifts via cascading of second order nonlinearities was directly applied to mode-locking. Using self-focusing by cascading in an LBO crystal, Cerullo *et al.* [33] were able to achieve Kerr-lens mode-locking (KLM) [125] of a Ti:Sapphire-pumped Nd:YAG laser shown in Fig. 29. Unlike the other techniques we have described, KLM relies on irradiance dependent cavity gain or loss that results from self-focusing in a nonlinear element [125]. The irradiances required for this effect in $\chi^{(3)}$ materials are large however, and therefore the technique is difficult to implement for pulsewidths longer than 1 ps [126]. Consequently, nonlinear phase shifts due to cascading are ideally suited to this application owing to the much larger $n_{2,\text{eff}}$. The KLM laser of [33] used a geometry quite similar to the diode-pumped laser of [100], but for the KLM laser, the mirror at the SHG end of the cavity is not dichroic, having $R_\omega = R_{2\omega} = 1$. This precludes any positive-feedback amplitude modulation due to the SHG crystal. Like some other KLM lasers [125], a slit was placed in the cavity to produce a nonlinear loss associated with the self-focusing. The mode-locking was found to depend strongly on the adjustment of the slit. This laser was made to operate at irradiances where η was only a few per cent. Under these conditions the low depletion approximation may be applied to find simple expressions for the double pass

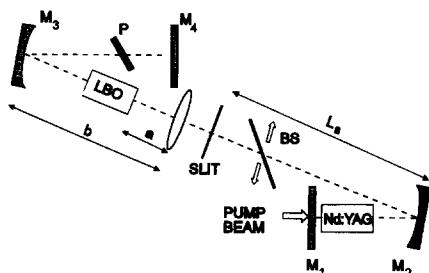


Figure 29 Configuration of cascaded Kerr-lens mode-locked Nd:YLF laser using a cw Ti:Sapphire pumped laser. (From [33].)

nonlinear phase shift, ϕ^{NL} :

$$\phi^{\text{NL}} \propto -(\kappa a_{\omega} L)^2 \left[2 \frac{\Delta k L - \sin \Delta k L}{(\Delta k L)^2} + \text{sinc}^2 \left(\frac{\Delta k L}{2} \right) \sin(\Delta \phi + \Delta k L) \right] \quad (17)$$

Optimum mode-locking was found to occur for $\Delta k L = \pi/2$ with $\Delta \phi$ adjusted to minimize the amount of SH remaining after double passing the crystal. Under these conditions, self-starting mode-locking was achieved, with 14 ps pulses at 0.5 W average power. To verify that the mode-locking was truly due to KLM, the mode size in the vicinity of the slit was measured to change by about 3% between the mode-locked and cw cases. In a subsequent paper, Cerullo *et al.* [114] showed that the pulse width may be reduced further by compensating for GVM in the SHG crystal. Using a birefringent plate to compensate the GVM, pulsewidths of 5.1 ps and 5.9 ps were obtained for Nd:YLF and Nd:YAG respectively.

The results of the Milan group [33, 99, 100, 114] demonstrate that there has been significant progress in the field of mode-locking via second order nonlinearities since its inception less than ten years ago. In particular, the application of cascading to Kerr-lens mode-locking [33] is particularly attractive for picosecond pulse generation, because for these pulsewidths, the use of $\chi^{(3)}$ is problematic. Similarly, the use of the Stankov Mirror in a flashlamp-pumped Nd:YLF laser [99] has several advantages (pulsewidth, stability, passivity) over acousto-optic active-mode-locking that is currently used in such laser systems.

3.6. Pulse compression

The mechanisms for pulse compression using second order nonlinearities are usually more complex than for mode-locking, as they may utilize the effects of GVD, as well as self-phase modulation (SPM) due to nonlinear phase shifts by cascading. The first suggestion of the use of second order media for extracavity pulse compression came in a theoretical paper by Wang and Draglia in 1990 [127]. This study primarily considered the effect of GVD on the efficiency of Type II phase-matched SHG in KDP for 1 ps Nd laser pulses. The authors showed that the effect of temporal walk-off can severely reduce the conversion efficiency under normal input conditions. However, it was noted that for this particular system, the group velocity at the second harmonic, v_3 , lies between that for the fundamental ordinary and extraordinary waves, v_o and v_e , i.e. $v_o < v_3 < v_e$. With this in mind, it was found that predelaying the extraordinary wave pulse could result in both an increase in SHG efficiency and a five-fold compression of the SH pulse. In this geometry, the extraordinary pulse passes through the ordinary pulse as they propagate through the crystal, while the SH pulse propagates with a group velocity that is the average of the two fundamental pulses. This form of compression was also predicted for the more general case of SFG by Stabinis *et al.* [128]. Their modelling showed that SF (or SH in the degenerate case) pulses could be produced from a KDP crystal with a 15-fold compression with respect to 3 ps input pulses from an Nd:YAG laser. Figure 30, taken from [128], shows the time dependence of the normalized irradiances of the waves to be summed, a_1 and a_2 , and the SF wave, a_3 , in the frame of reference of the SF pulse. Depletion of the trailing edge of a_1 (with lower group velocity) and the leading edge of a_2 (with higher group velocity) causes the temporal overlap to be limited and the shapes of a_1 and a_2 to be flattened. The extra bandwidth required for the compressed SF pulse comes from the strong saturation of the upconversion process.

This type of compression was later demonstrated experimentally by Wang and Luther-Davies, who showed compression of 1.2 ps Nd:YLF laser pulses to 250 fs at the second harmonic with a 1.4 ps pre-delay, in a 25 mm Type II KDP SHG crystal [129]. The effect of GVD actually allowed a

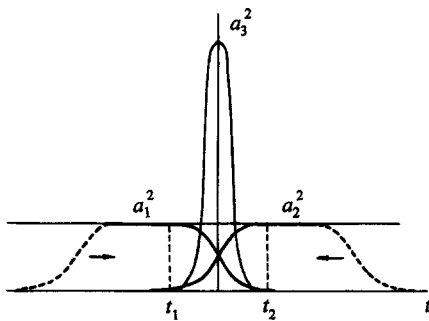


Figure 30 Temporal behaviour of normalized pulse irradiances in pulse compression via sum frequency generation, in the frame of reference of the SF pulse. a_1^2 and a_2^2 are the irradiances of the lower frequencies and a_3^2 is the SF irradiance. (From [128].)

peak power conversion efficiency of 240%. However, it was noted in the paper that the requirement on the group velocities combined with the phase-matching condition is quite specific to KDP at this wavelength, and hence not generally applicable to all SHG systems. In 1995, Umbrasas *et al.* reported a detailed experimental study of SH pulse compression of Nd:YAG laser pulses in KDP [130]. They demonstrated compression of 12 ps input pulses to 360 fs SH pulses in a 4 cm length KDP crystal with an 11 ps predelay between the 'o' and 'e' waves. It was shown both theoretically and experimentally that the optimum ratio of ordinary to extraordinary wave irradiances, I_o/I_e , is 1.3. Also, it was shown that the predelay for maximum compression is not the optimum for SHG efficiency. The compressed pulses have significant energy in satellite pulses, however, and the compression is not uniform across the spatial profile of the beams. Figure 31 shows an autocorrelation of the compressed SH pulse, measured at beam centre. It was suggested in [130] that the large satellite produced in the compressed pulse may not be detrimental to the application of pumping an OPO. At the same time, this was actually demonstrated by Danielus *et al.* [131] who used this type of compression to produce a short-pulse pump source for a BBO Optical Parametric Generator (OPG). It was shown that the satellites on the OPG output pulse were suppressed by a factor of $\sim 4 \times 10^4$ with respect to the compressed pump pulse. Using similar techniques, Nisoli *et al.* demonstrated pulse compression by SFG [132]. In this experiment, 160 fs signal and idler pulses from a Ti:Sapphire-pumped OPO at wavelengths of 1300 nm and 1950 nm, respectively, were mixed in a BBO crystal. With a predelay of around 200 fs, an SF pulsewidth of 34 fs was produced at a wavelength of 780 nm.

Self-compression of pulses was observed in a femtosecond OPO, by Laenen *et al.* [133]. When the BBO crystal was tuned near the degeneracy point, the OPO output pulsewidth

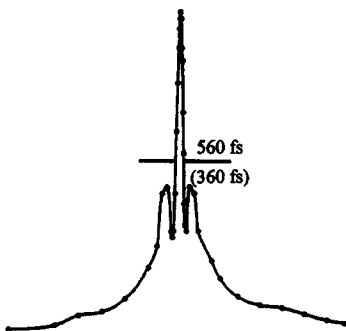


Figure 31 Autocorrelation of an SH pulse, compressed by SHG from a 12 ps Nd:YAG laser pulse in a 4 cm KDP crystal with an input irradiance of $I_o + I_e = 4.2 \text{ GW cm}^{-2}$. The number in parentheses is the pulse duration assuming a sech^2 pulse shape. (From [130].)

was reduced from over 200 fs to 65 fs. The mechanism suggested for this was chirp reversal of the idler pulses as a result of transference of the downchirp of the pump pulse through second order processes in the BBO crystal. The combination of the reversed chirp on the idler pulse and the normal dispersion on other intracavity elements results in the shortened output pulses. In a latter BBO-based OPO scheme, self-compression of pulses down to 50 fs was observed at a signal wavelength of 640 nm, far from degeneracy for this 400 nm pumped device [134]. It was shown later in [135] that this can be due to phase modulation by cascading associated with SHG of the signal wave in the BBO, as the phase-matching angles for the noncollinear parametric generation and collinear SHG of the idler are coincident at this particular wavelength.

Other methods of pulse compression using second order nonlinearities have also been demonstrated. The chirp enhancement in two-wave mixing, demonstrated by Danielus *et al.*, and described in section 3.3, was shown to provide an equally enhanced reduction of pulsewidth after compression by a grating pair, although the efficiency is small [92]. Pulse compression has also been observed by production of large spectral broadening through SPM in a DAN fibre and subsequent compression of the broadened pulse with a grating pair [136, 137]. In [137], a 39 fs pulse, at a wavelength of 623 nm from a colliding-pulse mode-locked dye laser, was compressed to 22 fs. The mechanism attributed to the SPM in [136] and [137] was a large third order nonlinearity, apparently neglecting the effects of cascading of second order nonlinearities which are very large in DAN [68]. A later paper from the same group [138] calculated that 100 W, 100 fs pulses could be compressed to around 10 fs based on the data taken in [136], but again, second order effects were neglected, so it is not clear if this can be realized experimentally.

4. Spatial solitons

The cascading nonlinearity can lead to self-trapped waves. The class of beams and pulses that propagate in the presence of diffraction and/or dispersion without spreading are called solitary waves. A special case is that of mathematical solitons which are obtained as the solutions of those very special evolution equations referred to as ‘completely integrable’. However, arbitrary small perturbations to such equations that arise in all real macroscopic systems break the delicate balance required for an equation to be a ‘soliton equation’. As a consequence, even though solitons are robust against certain types of perturbations, integrability is lost [139]. Therefore, except in rigorous mathematical contexts, it is accepted practice to use the term soliton in a broad sense to include also mathematical solitary waves and this terminology is used here. Such solitons can occur in many physical systems and their amplitude and phase distributions can be quite complex. The most common in optics in general, and in cascading in particular, are ‘bright’ and ‘dark’ solitons. Bright solitons consist of light waves which are strongly localized in space and/or time, whereas dark solitons consist of a dark region (hole) in a bright, constant, background light field with typically a π -phase change across the zero intensity point.

4.1. Simple models

The existence of quadratic spatial solitons was first discussed over 20 years ago [9, 12]. There are two limits of interest. In the limit in which the cascaded nonlinear phase shift closely mimics a third order nonlinearity (far from phase-matching), the types of solitons known for Kerr ($\chi^{(3)}$) nonlinearities are expected. In the cascaded case this region corresponds to very small harmonic conversion so only the fundamental carries significant power. By analogy, then, stable quadratic solitons are expected to exist in slab waveguides (1-D case) for positive nonlinearities. The self-focusing action of the nonlinear phase shift is the mechanism which allows the quadratic solitons to counteract spatial diffraction. Continuing the analogy to Kerr

nonlinearities, 2-D stable spatial solitons would not be expected to exist in the low SHG limit. However, they do exist as we shall discuss below.

One of the unique features of quadratic spatial solitons is that there are two strongly coupled fields which exchange energy with propagation distance. This energy exchange leads to another mechanism (in addition to self-focusing) for mutual self-trapping. There is a simple way to understand how this phenomenon can occur. (The more formal theory, etc., will be discussed in the next section.) Consider the coupled mode equations, including diffraction in one transverse dimension. For simplicity assume a 1-D slab waveguide with diffraction possible along the y -axis, i.e. the field amplitudes are functions of y and z and $a(z) \rightarrow a(y, z)$. The confinement along the x -axis is supplied by the index differences used to make the slab waveguide. The relevant coupled mode equations are:

$$\frac{d}{dz} a_1(y, z) + \frac{1}{2i k(\omega)} \frac{\partial^2}{\partial y^2} a_1(y, z) = -i\kappa(-\omega; 2\omega, -\omega) a_3(y, z) a_1^*(y, z) \quad (18)$$

$$\frac{d}{dz} a_3(y, z) + \frac{1}{2i k(2\omega)} \frac{\partial^2}{\partial y^2} a_3(y, z) = -i\kappa(-2\omega; \omega, \omega) a_1^2(y, z) \quad (19)$$

How these equations can lead to self-trapping can be explained with reference to the schematic in Fig. 32. Assume initially that there is no diffraction. Because $a_1^2(y, z)$ has a narrower spatial distribution along the y -axis than $a_1(y, z)$, then the generated SH via Equation 19 is narrower than the fundamental. When the fundamental is regenerated via $a_3(y, z) a_1^*(y, z)$, it is narrower than the original $a_1(y, z)$ not converted to SHG. Thus both the fundamental and harmonic can become progressively narrower due to the SHG process. However, all beams diffract on propagation. When the diffraction balances this narrowing effect, a spatial soliton can result in which both the fundamental and harmonic are mutually trapped. These waves are stable, i.e. small

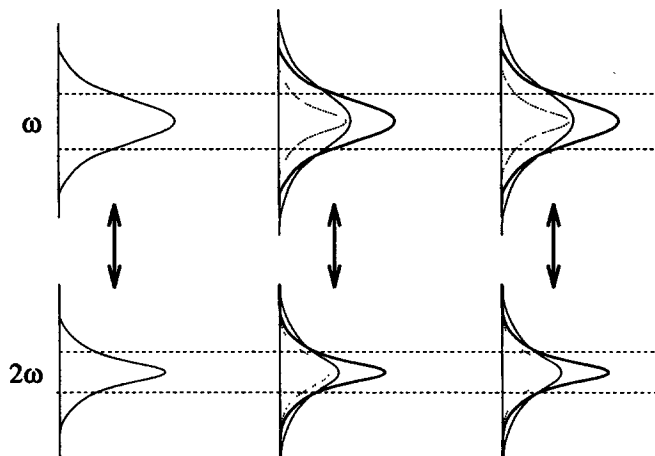


Figure 32 Illustration of how spatial beam overlap can lead to mutual beam trapping. The beams travel from left to right. Although shown separately, the fundamental (ω) and harmonic (2ω) are overlapped in space and have a common propagation axis. The lines with double-ended arrows represent power flow between the two beams. The regenerated fundamental (dotted line) is narrower in space than the non-converted and diffracted fundamental (light solid line) so that the total fundamental (heavy solid line) maintains its spatial profile with distance. The second harmonic maintains its spatial profile in the same way.

fluctuations in the input or propagation conditions do not destroy them. The key parameters are the parametric gain length $\propto [\kappa a_1(y, z)]^{-1}$ and the diffraction length. For the scenario described here, the parametric gain length, which is a measure of the distance over which the power can be efficiently exchanged between the two beams, should be of the order of, or shorter than, the characteristic diffraction distance for the two beams. Note that this argument extends directly to two transverse dimensions (and to the time domain) and hence this simple model would predict 2-D quadratic spatial solitons (and temporal solitons) which also consist of strongly coupled fundamental and harmonic beams. Note that in any real case, it is also necessary to consider the other mechanism, the self-focusing or self-defocusing due to the nonlinear phase shift.

4.2. Properties of $\chi^{(2)}$ solitons

4.2.1. Self-trapping in $\chi^{(2)}$ media

Self-focusing effects in SHG have been known for almost three decades in the regime where the wavevector mismatch is large so that the wave interaction yields an effective third order nonlinearity for the fundamental waves, as discussed in previous sections. This possibility was discussed by Ostrovskii in 1967 [6]. However, the extent of the self-focusing and its implications were not fully appreciated until recently.

The remarkable exception is the work of Karamzin and Sukhorukov in the 1970s. They recognized the potential of $\chi^{(2)}$ processes for supporting solitons under general phase-matching conditions, and performed analytical and numerical investigations to explore this possibility [9, 12]. Their work was not unnoticed and reappeared after the ‘wave’ of cascading in the 1990s reached the soliton area [140, 141]. The self-focusing potential of $\chi^{(2)}$ interactions was rediscovered a few years ago by a number of authors, not only in the regime where cascading mimics a cubic Kerr effect, but also near phase-matching [43, 142–145]. It is now known that solitons can exist in a wide variety of situations in terms of material and input light conditions: they form far from, near and at phase-matching, and in the presence of linear walk-off between the interacting waves. As discussed later, spatial solitons have been observed experimentally by Torruellas and coworkers, and by Schiek *et al.* [35, 146].

Self-trapping of light occurs when all the distances that govern the light evolution in the material are comparable, namely the diffraction or dispersion length, the walkoff length, and the nonlinear interaction length. To emphasize this point, it is useful to write the governing equations in normalized units scaled to these characteristic lengths. For the simplest case of Type I phase-matching SHG with diffraction allowed in 1-D (slab waveguide case), one gets

$$\begin{aligned} i \frac{\partial a_1}{\partial \xi} - \frac{r}{2} \frac{\partial^2 a_1}{\partial s^2} + a_1^* a_3 \exp(-i\beta\xi) &= 0 \\ i \frac{\partial a_3}{\partial \xi} - \frac{\alpha}{2} \frac{\partial^2 a_3}{\partial s^2} - i\delta \frac{\partial a_3}{\partial s} + a_1^2 \exp(i\beta\xi) &= 0 \end{aligned} \tag{20}$$

The details of the normalization, the meaning of the various parameters involved and their typical values in experimentally relevant situations are discussed in a number of papers [147–149]. To make contact with the preceding notation, the normalized wavevector mismatch $\beta = \text{sgn}(\Delta k) 2\pi l_{d1}/l_c$ where l_{d1} (l_{d2}) and l_c are the fundamental (second harmonic) diffraction length and the SHG coherence length respectively. The normalized coordinate along the propagation direction is $\xi = 2z/l_{d1}$ while the normalized transverse coordinate $s = y[k_1/2l_{d1}]^{1/2}$. For spatial solitons $r = -1$. The parameter $\alpha = -l_{d1}/l_{d2}$ and $\delta = \pm 2l_{d1}/l_w$ is a measure of the walk-off between the fundamental and harmonic beams where l_w is the walk-off length.

Note that walk-off is absent for propagation along the principal optical axes of the crystal. Similar but more complicated equations are obtained for Type II geometries, and for light propagation in bulk media [150]. The above equations also hold when pulsed light is injected into a channel waveguide or a fibre. Then the parameters r and α are given by the group-velocity dispersion at the fundamental and second harmonic frequencies, and δ stands for temporal pulse walk-off. Direct observation of temporal solitons in single-pass geometries appears to be difficult to achieve at present due to the lack of suitable materials that combine sufficiently high chromatic dispersion with low losses. Thus here we concentrate on spatial solitons.

The interacting waves exchange both energy and transverse phase-front information. When the material and input light conditions are chosen so that all of the characteristic lengths of the wave evolution are comparable, the precise form of the exchanged transverse phase-fronts becomes relevant. A soliton is formed when the mutually exchanged transverse phase-front shifts compensate for the linear spreading of the beams.

Significant simplification of the properties of the $\chi^{(2)}$ solitons can be made under certain conditions. The self-focusing nature of the wave mixing process in the limit of large phase-mismatch between the fundamental and harmonic waves ($\beta \gg 1$) and small conversion to the second harmonic results in governing equations which reduce approximately to the well-known nonlinear Schrödinger equation (NLSE)

$$i \frac{\partial a_1}{\partial \xi} + \frac{1}{2} \frac{\partial^2 a_1}{\partial s^2} + \frac{1}{\beta} |a_1|^2 a_1 \simeq 0 \quad (21)$$

In particular, for the case of 1-D self-trapping with a positive phase-mismatch, the $\chi^{(2)}$ solitons are similar to the NLSE solitons, and their dynamics resemble those of a perturbed NLSE in several ways [147]. However, the NLSE does not allow stable solitons for 2-D beams in bulk media and the implications of this fact to $\chi^{(2)}$ trapping in 2-D raise interesting questions. In fact the beam evolution in the $\chi^{(2)}$ medium quickly violates the approximations required to derive the NLSE, and $\chi^{(2)}$ stable soliton solutions exist even in the regime of large wavevector-mismatch. The limiting situation given by Equation 21 was noticed by a number of authors [43, 142, 143]. A significant contribution was made by Schiek who performed full numerical simulations for realistic waveguides and showed that Equation 21 was not just an elegant mathematical result but that solitons in that regime could indeed be observed experimentally [43].

However, an important point must be emphasized. Most of the solitons relevant to experimental study in quadratic media occur for small phase-mismatches, at exact phase-matching, and under other conditions where Equation 21 does not hold. Those solitons exhibit new properties, dynamics and other specific features. They have to be treated accordingly. In the last few years much progress has been made in the understanding of soliton formation and the main points will be reviewed in the following sections. To date, the efforts have been concentrated on second harmonic generation configurations and the extension to general three wave mixing interactions still remains to be done.

4.2.2. Families of solitons

The governing Equations 20 allow a variety of solitary wave solutions with bright, dark, bright-dark and exotic shapes. Owing to the space–time analogy of the equations, some results apply to both spatial and temporal solitons. The initial discussions will consider first the generic case of either spatial or temporal solitons and later the focus will be on spatial solitons.

A zero-parameter bright soliton solution, i.e., one that occurs for fixed values of all of the parameters involved, was found first by Karamzin and Sukhorukov [9]. It was rediscovered later by Hayata and Koshiba, Werner and Drummond, and Karpierz and Sypek [144, 145,

151]. In the normalized units of Equations 20, the solutions for the field amplitudes are given by

$$a_1 = 3\mu\sqrt{\alpha r} \operatorname{sech}^2(\sqrt{\mu}s) \quad a_3 = -3r\mu \operatorname{sech}^2(\sqrt{\mu}s) \quad (22)$$

and occur at the specific value of the phase-mismatch given by $\beta = -2\mu(\alpha - 2r)$ $\mu > 0$ being a free scaling parameter. Analytical, zero-parameter solutions for dark and exotically shaped solitons were also found by a number of authors who have to date presented the whole set of solitary waves having a reasonably simple shape [147, 151–154]. Several of these solutions only exist for the parameters appropriate to temporal solitons, but dark-like solutions also exist in the spatial case. However, as discussed later, they are unstable.

One-parameter families of stationary, bright soliton solutions with the soliton amplitude as the free parameter were found numerically for both 1-D and 2-D solitons [155–158]. Buryak and Kivshar have presented a comprehensive study and classification of 1-D solutions, including bright, dark and higher order solutions [155]. The set of solutions available for temporal solitons is in principle richer than for spatial solitons because of the variety of absolute values and signs of the GVD possible for the fundamental and second harmonic waves. Although dark spatial solitons even in an ideal flat background were found to be unstable due to the modulational instability of the background, Buryak and Kivshar discovered the existence of stable dark and twin-hole temporal solitons [54, 140, 159–161]. Higher-order, i.e., multiple-peaked solutions have been also investigated by Buryak and Kivshar, Mihalache and coworkers, and He and coworkers [155, 162, 163]. The solutions reported to date have been found to be unstable, even though some of them can exhibit weak instabilities, as discussed by Buryak [164]. Gap solitons which can exist in periodic structures under well-specified conditions have been also studied by Kivshar [165].

The families of bright spatial solitons in propagation geometries without walk-off exhibit important features. First, at phase-matching, the solutions exist for any value of the total power for both the 1-D and 2-D geometries, and all of the solitons are self-similar. In the case of 1-D solitons, they exist for any value of the wave power at positive phase-mismatch and exist above a threshold power at negative phase-mismatch [155–158]. Because low peak power solitons have a correspondingly large width, for a fixed input beam width there is always a threshold power for soliton formation. In the case of 2-D solitons in bulk media, they exist above a threshold power at both signs of the phase-mismatch. The threshold power required for trapping at negative phase-mismatch is larger than at positive phase-mismatch, consistent with the self-defocusing or self-focusing character of the wave interaction at very large phase-mismatch. At positive phase-mismatch, one finds that the threshold irradiance is given by $I_{\text{thr}} = \beta I_{\text{nl}}$, where I_{nl} is the critical power for collapse in the 2-D nonlinear Schrödinger equation. Figure 33 shows typical shapes of the 1-D spatial solitons for different values of the wavevector-mismatch [156]. Similar features are obtained for 2-D solitons. The partition of the total power between the fundamental and the second harmonic beams forming a soliton depends on the value of the wavevector-mismatch. This dependence is shown in Fig. 34 for a representative value of the total power, again for 1-D solitons [156]. More details about the properties of the bright spatial solitons can be found in references [155–158].

With the exception of special cases, linear walk-off between the waves that form a soliton introduces new physics into the process and modifies the families of solutions obtained in the absence of walk-off. Two-parameter families of solitons have been found under these conditions, and we shall return to this point below [166].

The excitation of bright solitons has been examined numerically for a wide variety of conditions [148–150]. One salient point that was found is that the excitation of solitons with arbitrary

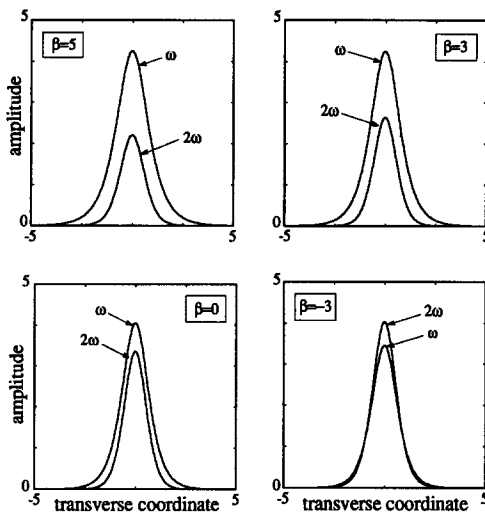


Figure 33 Typical field distributions for families of 1-D spatial solitons for different values of the linear wavevector mismatch β for a representative value of the soliton power. The plots show soliton fields for $\beta = 5, 3, 0, -3$. Similar shapes are obtained for 2-D solitons. (From [156].)

input beams always leads to oscillating states which consist of solitons and linear dispersive waves. The amplitude of the oscillations decreases as the waves propagate and shed power via dispersive waves. However, the rate of energy leakage is very small. Recently, Etrich and coworkers have studied this issue and have shown how the dispersive waves attached to the solitons and the internal dynamics of the solitons produce the oscillation process [167].

4.2.3. Stability

The stability on propagation of $\chi^{(2)}$ solitons has been studied by several authors and the stability issue seems to be well understood. Furthermore, important results about the effects that small perturbations have on the solitons are also being currently reported, even though the results reported to date cover only a small fraction of the issue.

An indication that stable $\chi^{(2)}$ solitons existed was given mathematically by Karamzin and coworkers and Kanashov and Rubenchik [9, 12, 140]. They showed that the Hamiltonian of the wave interaction is bounded from below and this result has implications to the existence of stable solutions [141]. More detailed studies along the same lines have been performed recently by Berge and coworkers and by Turitsyn [168, 169]. The existence of stable solitons under a wide variety of conditions is indeed supported by the results of a comprehensive series of numerical experiments of the soliton excitation problem [148–150].

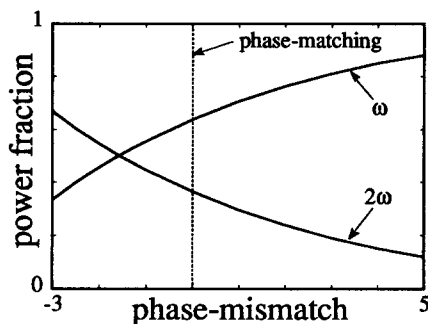


Figure 34 Distribution of the total soliton power between the fundamental and harmonic waves for a 1-D spatial soliton as a function of wavevector mismatch β for a fixed value of the total soliton power. (From [156].)

Once the families of the lowest-order stationary solutions are known in both 1-D and 2-D geometries, the question arises whether all members of the families are stable or not. This issue has been investigated by a number of authors for both the 1-D and 2-D cases [157, 158, 170–172]. In the absence of walk-off, all solutions at positive phase-mismatch and at exact phase-matching have been found to be stable. Some solutions which would be unstable have been found at negative phase-mismatch near the cutoff conditions for soliton existence, but above the threshold power for mutual trapping there is always a stable solution. A useful way to represent the soliton families is the Power–Hamiltonian diagrams employed by Akhmediev and coworkers for similar problems [173]. Figure 35 shows such a diagram for 1-D solitons at different values of the wavevector mismatch parameter β [171]. Dotted lines show unstable solutions, while continuous lines correspond to stable solitons [171]. The stable solutions occur at the absolute minimum of the Hamiltonian, hence they are stable in the Lyapunov sense [141]. In the presence of walk-off the families of solitons are modified and their stability has to be re-examined.

The effects of small losses on the solitons have been analysed by several authors [171, 174, 175]. When the losses are small over a diffraction length, the solitons evolve adiabatically following the amplitude–width relation of the family of solutions under investigation. At exact phase-matching, the relation $(\text{amplitude}) \times (\text{beam width})^2 = \text{constant}$ can be derived. Away from phase-matching the corresponding relation has been found numerically. Figure 36 shows this relation for the fundamental and harmonic associated with 2-D solitons [158]. The spatial width was found to be a smooth function of the amplitude. This means that the solitons broaden slowly as they lose total power, as was observed numerically by Hayata and Koshiba and studied analytically by Malomed and coworkers [174, 175]. When solitons are excited with arbitrary inputs, the radiative and reshaping and rephasing effects can dominate over the adiabatic effects due to losses.

The modulational instabilities of parametric processes in diffractive and dispersive scenarios have also been studied [54, 140, 159, 176]. In particular, Kanashov and Rubenchick found that the flat background of 1-D and 2-D spatial solitons is modulationally unstable in bulk, dispersive media, and that 3-D solitons (commonly referred to as light bullets) would be stable [140]. Trillo and coworkers investigated the modulational instabilities of both $\chi^{(2)}$ and $\chi^{(3)}$ solitons

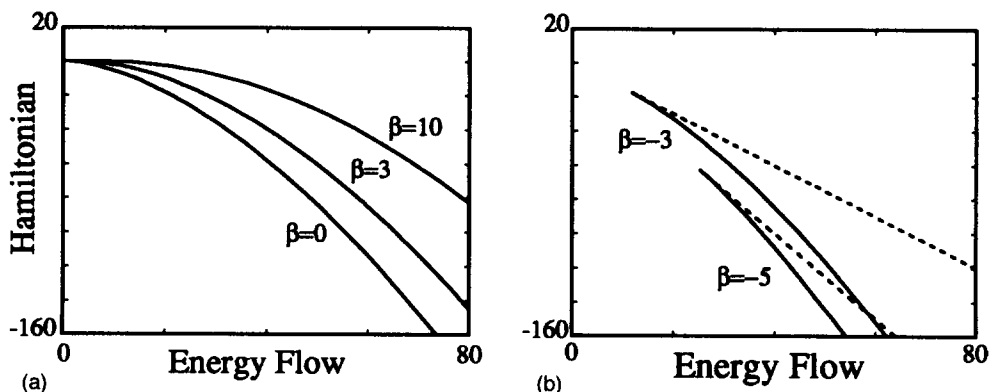


Figure 35 Hamiltonian versus power (energy flow) for families of 1-D spatial solitons. (a) For phase-matching ($\beta = 0$) and $\beta > 0$. (b) For $\beta < 0$. Continuous lines: stable solitons. Dashed lines: unstable solitons. Similar results are obtained for the 2-D case. (From [171].)

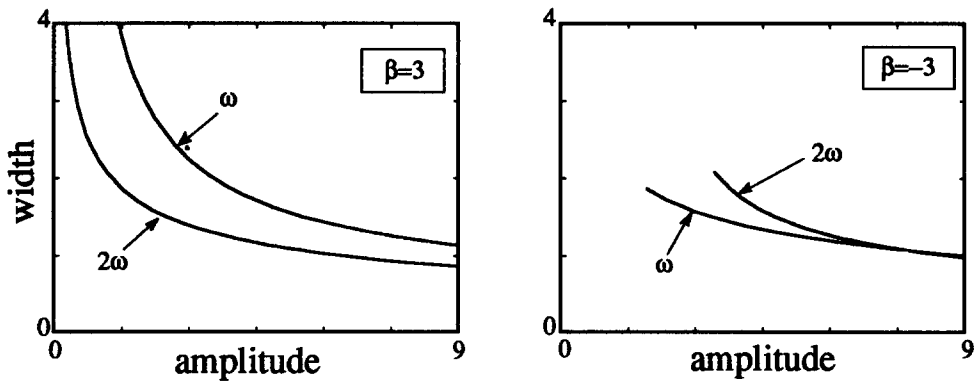


Figure 36 Width of the 2-D spatial solitons as a function of their amplitude, for both $\beta > 0$ and $\beta < 0$. 1-D spatial solitons exhibit similar trends (from [158]).

due to the competition of quadratic and cubic nonlinearities [177]. The effects introduced in the $\chi^{(2)}$ solitons by the presence of $\chi^{(3)}$ nonlinearities have also been studied by other authors and analytical solitary wave solutions in the presence of both quadratic and cubic nonlinearities have been found [155, 178, 179].

4.2.4. Walking solitons

By their very nature, solitons in quadratic nonlinear media exist by virtue of the mutual trapping of several waves, namely the fundamental and second harmonic waves in the case of SHG solitons. Generally speaking, at low irradiances the waves that constitute the soliton propagate at different velocities/directions, and hence they walk off from each other. This feature has important experimental implications when it comes to the actual excitation of solitons. It not only offers possibilities for novel applications, it also poses new challenges to the theoretical understanding of soliton formation.

When a soliton is formed, the waves mutually trap and drag each other, and therefore propagate as a single entity, i.e. bound together. These are ‘walking’ solitons. This phenomenon is somewhat analogous to Vector or Manakov spatial solitons, or temporal solitons in fibres in which two orthogonal polarizations in cubic nonlinear media are mutually trapped and co-propagate [37, 38, 180, 181]. However in those cases solitons with a single polarization do exist, whereas in the case of $\chi^{(2)}$ solitons all of the interacting waves are needed to form a soliton. Figure 37 shows the

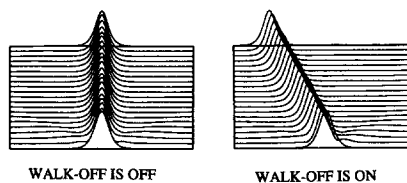


Figure 37 The propagation of the fundamental beam component of a 1-D spatial soliton with and without Poynting vector beam walk-off by the second harmonic beam (not shown here). Without walk-off, both beams propagate normal to the entrance face. With walk-off, the fundamental beam is bound to the harmonic and is deflected to the left, i.e. it is dragged by the harmonic into a new propagation direction.

representative effects of walk-off on the trapping process. Detailed studies of the dynamics of soliton formation in the presence of walk-off in both planar waveguides and bulk media have been reported [148, 149]. Once again the focus has been on spatial solitons but most issues studied have their temporal counterparts. Notice that walk-off is an unavoidable ingredient of $\chi^{(2)}$ spatial solitons in geometries based on birefringent phase-matching.

Suppression of the linear walk-off by the nonlinear dragging of the interacting beams allows the control of the output position of the beams at the end of the $\chi^{(2)}$ crystal by modifying the transverse velocity of the individual constituents of the solitons excited. This can be done in different ways by controlling the material and input wave conditions. The process leads to beam steering, pointing, scanning and switching, all of which have been investigated both theoretically and experimentally [182–185]. Also, as a consequence of the mutual dragging of the interacting beams, the effective walk-off experienced by a given soliton depends on its amplitude. Under appropriate conditions in planar waveguides, this leads to the controllable self-splitting of beams into several solitons, a process that might be referred to as eigenvalue switching [186].

A good understanding of the process of mutual dragging has been obtained by considering the solitons as a single entity, i.e., using their particle-like nature, and analysing their formation in terms of the conserved quantities of the beam evolution. In particular, one readily finds that the transverse velocity of the ‘walking’ solitons is given by

$$\nu \simeq -\delta \frac{I_3}{I} + \frac{J}{I} \quad (23)$$

where $I = I_1 + I_3$ [182]. The quantity J is the transverse momentum of the soliton parallel to the entrance face of the medium and is basically determined by its phase-front [182]. This expression shows how the dragging can be controlled by the input light and material conditions, in terms of global phases, phase-front and beam shapes, total and relative powers of the input waves, wavevector-mismatch and linear walk-off.

In the presence of walk-off, the walking solitons exhibit specific features different from just a phase-front tilt of the nonlinear Schrödinger equation solitons. This is similar to solitons of other non-Galilean invariant equations, such as gap solitons or walking vector solitons in birefringent cubic nonlinear media [187, 188]. Families of stationary walking solitons have been discovered recently [166]. They have been found to form two-parameter families as they exist for different soliton energies and transverse velocities for a given wavevector mismatch. Much work remains to be done to understand fully the properties of all the families of walking solitons.

4.2.5. Soliton interactions

As discussed above, $\chi^{(2)}$ solitons form two-parameter families of solutions and they are stable on propagation in the Lyapunov sense. However, they are not inverse scattering solitons, i.e., they are not obtained as the soliton solutions of a so-called completely integrable equation. This is in contrast to, e.g., the solitons governed by the nonlinear Schrödinger equation which, under ideal conditions, models the wave propagation in cubic nonlinear media in appropriate waveguide geometries. This has the consequence that the interactions between $\chi^{(2)}$ solitons do not enjoy the unique features that only hold for mathematical solitons. Rather, generally speaking, in the interaction between $\chi^{(2)}$ solitons one has to expect behaviour typical of non-integrable systems. An example of this case is wave propagation in saturable cubic nonlinear media. Also, because parametric interactions in quadratic nonlinear media are highly

sensitive to the relative phases between the interacting fields, the phase difference between two colliding solitons plays an important role in their interaction.

The interactions between 1-D solitons have been investigated by Baboiu *et al.* and Etrich *et al.* by means of numerical experiments [189, 190]. The results, discussed later, confirmed the above expectations and showed a rich dynamical behaviour. Buryak *et al.* have shown some results for 2-D soliton interactions [157]. The results reported were qualitatively similar to those for 1-D geometries, even though in general different dynamics are expected. Finally, Clausen *et al.* have used a perturbative scheme for the collective coordinates of the solitons to gain insight into the dynamics of their collisions [191]. The outcome provides a simple qualitative picture of the soliton interaction.

Although the result of a soliton interaction depends a great deal on the various specific parameters involved, a few general conclusions primarily for 1-D solitons have been reached, as follows. (1) In-phase, parallel equal-amplitude solitons attract each other and eventually fuse into a single beam. Clausen and coworkers found that the fusion distance increases exponentially with the initial soliton separation [191]. (2) Baboiu and coworkers found that parallel equal-amplitude solitons with a phase difference eventually repel each other above a threshold phase difference [189]. The threshold phase difference even vanishes in some cases and in general is a function of the various parameters involved, namely the wavevector-mismatch, input beam shape and power, radiation present in the input beams, and so on. (3) Solitons colliding at large enough angles, i.e., with large transverse velocities, were found to pass through each other without significant noticeable changes. (4) Solitons having different amplitudes have been observed to interact weakly because the nonlinear phase-shift acquired by one soliton is different from that of the second soliton. (5) At large wavevector-mismatch the $\chi^{(2)}$ solitons resemble perturbed nonlinear Schrödinger equation solitons and so do their interactions. This regime was investigated by Etrich and coworkers [190].

Some of the above features are summarized in the plots in Fig. 38. The results available to date reveal only the surface of the problem and much work needs to be done to understand fully the details of the soliton interactions. That is particularly true for 2-D solitons, for which only a few results are known.

4.2.6. Beyond cascading

Before ending this section, it is worth recalling that the formation of optical solitons in quadratic nonlinear media through cascading can potentially have important implications not only for nonlinear optics, but also for other branches of nonlinear science. This is possible because parametric, resonant three wave mixing processes play an important role in many branches of physics and technology, such as plasma physics, fluid dynamics, water and acoustic waves, or electronic parametric amplifiers [192].

In many situations of interest, dispersive effects take place on a much longer time or space scale than the nonlinear effects. In those cases, the corresponding governing equations have a universal

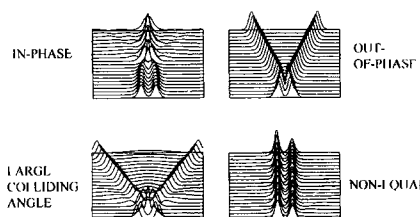


Figure 38 Typical interactions between 1-D spatial solitons under a variety of interesting input conditions.

nature, analogous to the nonlinear Schrödinger equation or the Korteweg–de Vries equation, and they have been extensively investigated for more than three decades. Under such conditions, much progress can be made by using analytical tools, including the inverse scattering transform method [193–195]. However, the formation of stable multidimensional optical solitons through cascading shows that in other physical settings, when the dispersive and nonlinear scale lengths are comparable, the parametric interactions of intense waves may exhibit a much richer variety of phenomena than previously believed. The potential of cascading to reveal some of those universal features needs to be exploited.

4.3. Experiments on spatial solitary waves

There have been a limited number of experiments reported on quadratic spatial solitary waves. Both the 1-D and 2-D cases have been investigated.

4.3.1. 1-D spatial solitons

Spatial solitary waves which are free to diffract in one transverse dimension have been successfully launched in LiNbO₃ slab waveguides [146]. The same waveguides as described in section 2.2 were used so that minimal SHG was involved (checked to be less than a few per cent) with still a reasonable effective nonlinearity [146]. As a result the solitary wave resembles a Kerr spatial soliton to a good approximation. In the experiment, a circular and cylindrical lens pair were used to end-fire couple a 70 μm wide beam at 1320 nm into the slab waveguide. The beam irradiance at the output face was imaged on to a camera and the results, as a function of input power, r , are shown in Fig. 39. At low powers the beam diffracts considerably in the sample which was about 3 diffraction lengths long. With increasing power self-focusing occurs. Once a beam width comparable to the input beam width was achieved, a further increase in input power has little effect on the output beam width, verifying that a spatial soliton was indeed obtained. Furthermore, the agreement with theory was found to be excellent.

4.3.2. 2-D spatial solitary waves

The formation of spatial solitary waves with two transverse dimensions has been demonstrated by Torruellas and colleagues in a relatively complicated interaction geometry [35]. Type II phase-matching in a 0.5 cm KTP crystal was used with fundamental radiation at 1064 nm. This case requires two fundamental input beams, one ordinary and one extraordinary with spatial walk-off between them. The two input fundamentals were focused to a radius of 20 μm at the crystal entrance face and the beam at the output face, 5 diffraction lengths away, was focused on to a vidicon camera.

The output beam profile of the fundamental is shown in Fig. 40 for three different input irradiances [35]. At low irradiances, the beam diffracts in space, as expected. Above a threshold

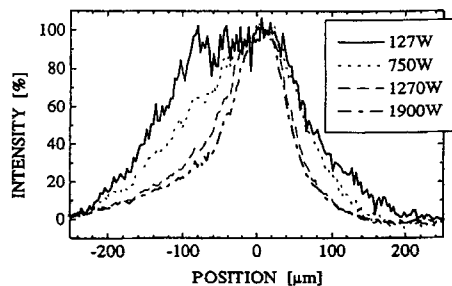


Figure 39 The in-plane spatial irradiance profile of the output beam from a slab LiNbO₃ waveguide for different input powers. (From [145].)

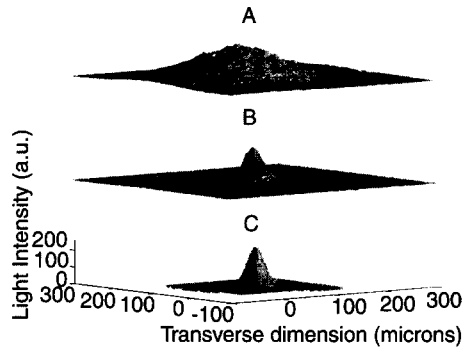


Figure 40 The fundamental beam profile output from phase-matched KTP for three different input beam irradiances. Below threshold the beam diffracts, and at and above threshold a solitary wave beam is formed in the crystal. 1064 nm, 30 ps pulses were used in a 1 cm KTP crystal. (From [35].)

of approximately 10 GW cm^{-2} , the beam narrows to about $12.5 \mu\text{m}$ and remains at this value for subsequent increase in power up to 100 GW cm^{-2} , see Fig. 41. The second harmonic beam diameter undergoes the same transformation. Notice that this threshold value corresponds to an input beam formed only by the fundamental wave. If both fundamental and second harmonic waves would be supplied at the entrance face of the crystal, a significant reduction of the power threshold would be obtained. Thus 2-D spatial solitary waves were observed.

There were other interesting features observed in this experiment. First, above the solitary wave locking threshold all three beams, the two fundamentals and the harmonic propagate together in space. That is, above the solitary wave locking threshold walk-off is overcome. Second, as shown in the inset of Fig. 41, solitary waves are generated even with multi- π phase-mismatches of either sign. That is, the process ‘pulls itself’ on to phase-matching by the generation of the spatial solitary waves. Note that for positive phase-mismatch, the self-focusing action associated with a positive nonlinear phase shift decreases the threshold for solitary wave formation, and vice versa for the negative phase-mismatch. This clearly shows that there are two distinct mechanisms, one due to the spatial narrowing associated with the power exchange via the

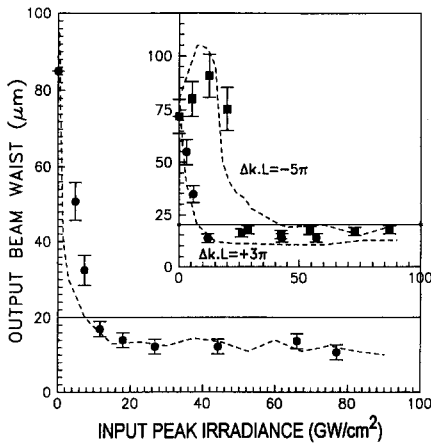


Figure 41 The output fundamental 2-D beam width versus peak input fundamental irradiance on phase-matching (lower curve), a phase mismatch $\Delta kL = 3\pi$ (inset, solid circles) and a phase mismatch $\Delta kL = -5\pi$ (inset, solid squares). 1064 nm, 30 ps pulses were used in a 1 cm KTP crystal. (From [35].)

coupled mode equations discussed above, and the second due to the curvature of the wavefront introduced by the nonlinear phase shift. Third, the fraction of the power in the SHG and fundamental beams in the solitary wave remains approximately constant as the input irradiance is increased.

Further experiments showed that this beam trapping is a rich phenomenon [183, 184]. By changing the relative phase between the fundamentals and a seeding second harmonic beam, it proved possible to change the trapping direction in space [183]. The extrema are defined by the directions which one of the beams would follow when excited singly. It has also been demonstrated that the direction of the trapped beam can be controlled by varying the relative irradiance of the two fundamental beams, more useful than varying the phase which is a difficult variable to control [184]. An example is shown in Fig. 42 where the trapped output beam for three different irradiance ratios between the two fundamentals is plotted. By placing apertures to intercept the different extreme beam positions, an all-optical switch can be implemented and indeed switching action was demonstrated. The beauty of this scheme is that the relative phase does not need to be changed.

The research into spatial solitary waves has continued at CREOL and here we give some new results which will be reported in detail elsewhere [196]. An example, shown in Fig. 43, is the beam transformation which occurs for elliptical input beams. Two different kinds of phenomena are observed. At low enough input powers, but above a well-defined threshold (which varies inversely with ellipticity), the beam evolves into a cylindrically symmetric spatial solitary wave. The fraction of the input power which is trapped by the solitary wave decreases with increasing ellipticity. At very high input irradiances, the input breaks up into a 'string' of spatial solitary waves, as seen in Fig. 43d. These phenomena are due to the modulational instability of the input beam, and the details of the beam splitting are not fully understood at present.

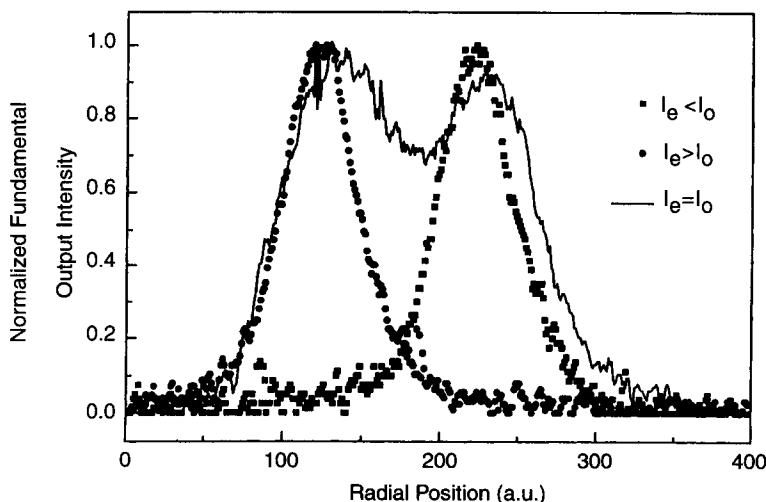


Figure 42 The beam profiles output from a 1 cm KTP crystal near Type II phase-matching for three different irradiances of the two orthogonally polarized fundamental beams: circles: $I_1 > I_2$; continuous curve: $I_1 \simeq I_2$; squares: $I_2 > I_1$. (From [183].)

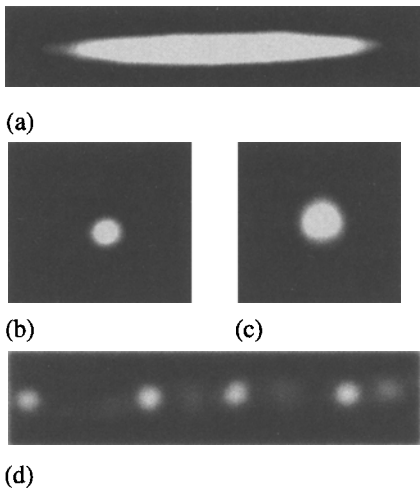


Figure 43 Solitary wave effects for an elliptical input beam (a, top). The middle results (b, c) are for irradiances just above the solitary wave threshold which shows a circular beam output: left-hand side – right at the output crystal face; right-hand side – 0.5 mm from exit face. The bottom (d) shows a line of spatial solitary waves generated at high input irradiances. (From [196].)

5. Summary

We have presented an overview of the field which has taken on the name ‘cascading’. It represents a rebirth of interest in $\chi^{(2)}$ phenomena beyond the usual goals of generating new wavelengths as efficiently as possible. In fact this field has proven to be rich in interesting phenomena, many of which were initially considered in early days of nonlinear optics, but never exploited beyond general theoretical predictions. Some aspects of cascading have evolved independently of one another over the last five years and one of our goals was to bring together all of the different research directions under one unified discussion. The two major themes appear to be the existence of large nonlinear phase shifts in the parametric mixing process and their ensuing applications, and the formation of a rich variety of solitary waves. Given the rapid growth over the last five years, one can expect many new and exciting developments over the next five years.

Acknowledgements

Many colleagues have contributed to our understanding of cascading. Their work has formed the core of this article and we wish to acknowledge their contributions: Eric VanStryland, William Torruellas, Roland Schiek, Gaetano Assanto, Curtis Menyuk, Gijs Krijnen, Christian Bosshard, Mansoor Sheik-Bahae, Joe Zyss, Peter Vidakovic, Marc DeMichelli, Wolfgang Sohler, Richard DeSalvo, Mike Sundheimer, Yongsoon Baek, Brian Lawrence, Daniel Baboiu, Carlos G. Treviño-Palacios, Pascal Baldi and Zuo Wang. The authors also wish to acknowledge and thank ARPA, ARO, NSF and AFOSR for supporting various aspects of the cascading research at CREOL. Lluís Torner also acknowledges the generous support of the Spanish government through DGICYT.

References

1. J. A. ARMSTRONG, N. BLOEMBERGEN, J. DUCUING and P. S. PERSHAN, *Phys. Rev.* **127** (1962) 1918–39.
2. Y. R. SHEN, *Principles of Nonlinear Optics* (Wiley, New York, 1984).
3. F. A. HOPF and G. I. ROSE, *Applied Classical Electrodynamics, Vol. 2: Nonlinear Optics* (Wiley, New York, 1986).
4. R. W. BOYD, *Nonlinear Optics* (Academic Press, Boston, 1992).
5. P. N. PRASAD and D. J. WILLIAMS, *Introduction to Nonlinear Optical Effects in Molecules and Polymers* (Wiley, New York, 1991) Chapters 6 and 9.
6. L. A. OSTROVSKII, *JETP Lett.* **5** (1967) 272–5.

7. J. P. COFFINET and F. DE MARTINI, *Phys. Rev. Lett.* **22** (1969) 60–4.
8. CHR. FLYTZANIS and N. BLOEMBERGEN, *Quant. Electron.* **4** (1976) 271–300; CHR. FLYTZANIS, in *Quantum Electronics*, edited by H. Rubin and C. L. Tang (Academic Press, New York, 1975), Vol. 1, Part A.
9. Y. N. KARAMZIN and A. P. SUKHORUKOV, *JETP Lett.* **20** (1974) 339–42.
10. T. K. GUSTAFSON, J.-P. E. TARAN, P. L. KELLEY and R. Y. CHIAO, *Opt. Commun.* **2** (1970) 17–21.
11. D. N. KLYSHKO and B. F. POLKOVNIHOV, *Sov. J. Quant. Electron.* **3** (1972) 324–6.
12. YU. N. KARAMZIN and A. P. SUKHORUKOV, *Zh. Eksp. Teor. Phys.* **68** (1975) 834–40 (*Sov. Phys.-JETP* **41** (1976) 414–20).
13. K. JAIN and G. W. PRATT JR., *Appl. Phys. Lett.* **28** (1976) 719–21.
14. R. NAKACH and H. WILHELMSSON, *Phys. Rev. A* **14** (1976) 451–6.
15. N. B. BARANOVA and B. YA. ZEL'DOVICH, *Sov. Phys. Dokl.* **27** (1982) 222–3; *Dokl. Akad. Nauk SSSR* **263** (1982) 325–7.
16. J.-M. R. THOMAS and J.-P. E. TARAN, *Opt. Commun.* **4** (1972) 329–34.
17. R. C. ECKARDT and J. REINTJES, *IEEE J. Quant. Electron.* **20** (1984) 1178–87.
18. J. T. MANASSAH, *J. Opt. Soc. Am. B* **4** (1987) 1235–40.
19. H. J. BAKKER, P. C. M. PLANKEN, L. KUIPERS and A. LAGENDIJK, *Phys. Rev. A* **42** (1990) 4085–101.
20. E. YABLONOVITCH, C. FLYTZANIS and N. BLOEMBERGEN, *Phys. Rev. Lett.* **29** (1972) 865–8.
21. S. A. AKHMANOV, A. N. DUBOVIK, S. M. SALTIEL, I. V. TOMOV and V. G. TUNKIN, *JETP Lett.* **20** (1974) 117–18; *Zh. ETF Pis. Red.* **20** (1974) 264–8.
22. S. A. AKHMANOV, L. B. MEISNER, S. T. PARINOV, S. M. SALTIEL, I. V. TOMOV and V. G. TUNKIN, *Sov. Phys. JETP* **46** (1977) 898–907; *Zh. Eksp. Teor. Fiz.* **73** (1977) 1710–28.
23. M. ZGONIK and P. GUNTER, *Ferroelectrics* **126** (1992) 33–8.
24. G. R. MEREDITH, *Phys. Rev. B* **24** (1981) 5522–32.
25. N. R. BELASHENKOV, S. V. GAGARSKII and M. V. INOCHKIN, *Opt. Spectrosc.* **66** (1989) 806–808.
26. R. DESALVO, D. J. HAGAN, M. SHEIK-BAHAE, G. STEGEMAN and E. W. VAN STRYLAND, *Opt. Lett.* **17** (1992) 28–30.
27. G. I. STEGEMAN and E. M. WRIGHT, *J. Optical and Quant. Electron.* **22** (1990) 95–122.
28. I. LEDOUX, C. LEPERS, A. PÉRIGAUD, J. BADAN and J. ZYSS, *Opt. Commun.* **80** (1990) 149–54.
29. S. R. MARDER, J. W. PERRY and C. R. YAKYMYSHYN, *Chem. Mater.* **6** (1994) 1137–47.
30. CH. BOSSHARD, K. SUTTER, R. SCHLESSER and P. GUNTER, *J. Opt. Soc. Am. B* **10** (1993) 867–85.
31. M. M. FEJER, G. A. MAGEL, D. H. JUNDT and R. L. BYER, *IEEE, J. Quant. Electron.* **28** (1992) 2631–54.
32. K. A. STANKOV and J. JETHWA, *Opt. Commun.* **66** (1988) 41–6.
33. A. CERULLO, S. DE SILVESTRI, A. MONGUZZI, D. SEGALA and V. MAGNI, *Opt. Lett.* **20** (1995) 746–8.
34. J. S. AITCHISON, A. M. WEINER, Y. SILBERBERG, M. K. OLIVER, J. L. JACKEL, D. E. A. LAIRD, E. M. VOGEL and P. W. E. SMITH, *Opt. Lett.* **15** (1990) 471–3.
35. W. E. TORRUELLAS, Z. WANG, D. J. HAGAN, E. W. VAN STRYLAND, G. I. STEGEMAN, L. TORNER and C. R. MENYUK, *Phys. Rev. Lett.* **74** (1995) 5036–9.
36. G. C. DURREE JR., J. L. SHULTZ, G. J. SALAMO, M. SEGEV, A. YARIV, B. CROSIGNANI, P. DI PORTO, E. J. SHARP and R. R. NEURGAONKAR, *Phys. Rev. Lett.* **71** (1993) 533–6.
37. J. U. KANG, G. I. STEGEMAN, J. S. AITCHISON and N. AKHMEDIEV, *Phys. Rev. Lett.* **76** (1996) 3699–702.
38. J. S. AITCHISON, J. U. KANG, G. I. STEGEMAN, N. N. AKHMEDIEV and E. A. OSTROVSKAYA, Observation of vector spatial solitons, unpublished.
39. G. I. STEGEMAN, R. SCHIEK, L. TORNER, W. TORRUELLAS, Y. BAEK, D. BABOIU, Z. WANG, E. VAN STRYLAND, D. HAGAN and G. ASSANTO, in *Novel Optical Materials and Applications*, edited by I. C. Khoo and F. Simoni (Wiley Interscience, New York, 1995), p. 49.
40. CH. BOSSHARD, *Adv. Mater.* **8** (1996) 385–397.
41. G. I. STEGEMAN, M. SHEIK-BAHAE, E. W. VAN STRYL and G. ASSANTO, *Opt. Lett.* **18** (1993) 13–15.
42. P. PLISZKA and P. P. BANERJEE, *J. Modern Optics* **40** (1993) 1909–16.
43. R. SCHIEK, *J. Opt. Soc. Am. B* **10** (1993) 1848–1854.
44. L. KADOR, *Appl. Phys. Lett.* **66** (1995) 2938–9.
45. B. F. LEVINE, C. G. BETHEA, C. D. THURMOND, R. T. LYNCH and J. L. BERNSTEIN, *J. Appl. Phys.* **50** (1979) 2523–7.
46. B. LAWRENCE, M. CHA, J. U. KANG, W. TORRUELLAS, G. I. STEGEMAN, G. BAKER, J. METH and S. ETEMAD, *Electron. Lett.* **30** (1994) 447–8.
47. S. TRILLO, S. WABNITZ, R. CHISARI and G. CAPPELLINI, *Opt. Lett.* **17** (1992) 637–9.
48. G. ASSANTO, G. I. STEGEMAN, M. SHEIK-BAHAE and E. W. VAN STRYLAND, *Appl. Phys. Lett.* **62** (1993) 1323–5.

49. D. J. HAGAN, M. SHEIK-BAHAE, Z. WANG, G. STEGEMAN, E. W. VAN STRYLAND and G. ASSANTO, *Opt. Lett.* **19** (1994) 1305–7.
50. P. ST. J. RUSSELL, *El. Lett.* **29** (1993) 1228–9; P. ST. J. RUSSELL, *IEEE J. Quant. Electron.* **27** (1991) 830–5.
51. G. ASSANTO, G. I. STEGEMAN, M. SHEIK-BAHAE and E. W. VAN STRYLAND, *IEEE J. Quant. Electron.* **31** (1995) 673–81.
52. L. LEFORT and A. BARTHELEMY, *Opt. Commun.* **119** (1995) 163–6.
53. A. E. KAPLAN, *Opt. Lett.* **18** (1993) 1223–5.
54. S. TRILLO and P. FERRO, *Opt. Lett.* **20** (1995) 438–40.
55. D. HUTCHINGS, J. S. AITCHISON and C. N. IRONSIDE, *Opt. Lett.* **18** (1993) 793–5.
56. A. L. BELOSTOTSKY, A. S. LEONOV and A. V. MELESHKO, *Opt. Lett.* **19** (1994) 856–8.
57. G. ASSANTO, I. TORELLI and S. TRILLO, *Opt. Lett.* **19** (1994) 170–2.
58. G. ASSANTO, *Opt. Lett.* **20** (1995) 1595–7.
59. G. ASSANTO and I. TORELLI, *Opt. Commun.* **119** (1995) 143–8.
60. A. KOPYAKOV, U. PESCHEL, R. MUSCHALL, G. ASSANTO, V. P. TORCHIGIN and F. LEDERER, *Opt. Lett.* **20** (1995) 1686–8.
61. A. KOPYAKOV, U. PESCHEL and F. LEDERER, *Opt. Commun.* **124** (1996) 184–94.
62. G. ASSANTO, I. TORELLI and S. TRILLO, *Electron. Lett.* **30** (1994) 733–5.
63. S. TRILLO and G. ASSANTO, *Opt. Lett.* **19** (1994) 1825–7.
64. F. HACHE, A. ZÉBOULON, G. GALLOT and G. M. GALE, *Opt. Lett.* **20** (1995) 1995–8.
65. H. TAN, G. P. BANFI and A. TOMASELLI, *Appl. Phys. Lett.* **63** (1993) 2472–5.
66. J. R. DESALVO, 'On nonlinear refraction and two-photon absorption in optical media', PhD thesis (1993) Un. Central Florida, Chapter 7.
67. S. NITTI, H. M. TAN, G. P. BANFI and V. DEGIORGIO, *Optics Commun.* **106** (1994) 263–8.
68. D. Y. KIM, W. E. TORRUELLAS, J. KANG, C. BOSSHARD, G. I. STEGEMAN, P. VIDAKOVIC, J. ZYSS, W. E. MOERNER, R. TWIEG and G. BJORKLUND, *Opt. Lett.* **19** (1994) 868–70.
69. M. I. SUNDHEIMER, CH. BOSSHARD, E. W. VAN STRYLAND, G. I. STEGEMAN and J. D. BIERLEIN, *Opt. Lett.* **18** (1993) 1397–9; M. L. SUNDHEIMER, A. VILLENEUVE, G. I. STEGEMAN and J. D. BIERLEIN, *Electron. Lett.* **30** (1994) 1401–2.
70. R. SCHIEK, M. L. SUNDHEIMER, D. Y. KIM, Y. BAEK, G. I. STEGEMAN, H. SUCHE and W. SOHLER, *Opt. Lett.* **19** (1994) 1949–51.
71. G. J. M. KRIJNEN, W. TORRUELLAS, G. I. STEGEMAN, P. V. LAMBECK and H. J. W. M. HOEKSTRA, *IEEE J. Quant. Electron.* **32** (1996) 729–38.
72. CH. BOSSHARD, R. SPEITER, M. ZGONIK and P. GUNTER, *Phys. Rev. Lett.* **74** (1995) 2816–19.
73. P. UNSBO, *J. Opt. Soc. Am. B* **12** (1995) 43–8.
74. M. ZGONIK and P. GÜNTER, *J. Opt. Soc. Am. B* **13** (1996) 570–6.
75. G. I. STEGEMAN and A. MILLER, in *Photonic Switching, Vol. I*, edited by J. Midwinter (Academic Press, Orlando, 1992) pp. 81–146.
76. R. SCHIEK, *Opt. Quantum Electron.* **26** (1994) 414–31.
77. C. N. IRONSIDE, J. S. AITCHISON and J. M. ARNOLD, *IEEE J. Quant. Electron.* **29** (1993) 2650–4.
78. G. ASSANTO, A. LAURETI-PALMA, C. SIBILIA and M. BERTOLOTTI, *Opt. Commun.* **110** (1994) 599–603.
79. M. PICCIAU, G. LEO and G. ASSANTO, *J. Opt. Soc. Am. B* **13** (1996) 661–70.
80. Y. BAEK, R. SCHIEK and G. I. STEGEMAN, *Opt. Lett.* **20** (1995) 2168–70.
81. Y. BAEK, R. SCHIEK, G. KRIJNEN, G. I. STEGEMAN, I. BAUMANN and W. SOHLER, *Appl. Phys. Lett.* **68** (1996) 2055–7.
82. R. SCHIEK, Y. BAEK, G. KRIJNEN, G. I. STEGEMAN, I. BAUMANN and W. SOHLER, *Opt. Lett.* **21** (1996) 940–2.
83. H. M. GIBBS, *Optical Bistability: Controlling Light by Light* (Academic Press, New York, 1985).
84. C. RICHY, K. I. PETSAS, E. GIACOBINO, C. FABRE and L. LUGIATO, *J. Opt. Soc. Am. B* **12** (1995) 456–61.
85. Z. Y. OU, *Opt. Commun.* **124** (1996) 430–7.
86. A. G. WHITE, J. MLYNEK and S. SCHILLER, *Europhysics Lett.* **35** (1996) 425–30.
87. R. REINISCH, E. POPOV and M. NEVIERE, *Opt. Lett.* **20** (1995) 854–6.
88. R. REINISCH, M. NEVIERE and E. POPOV, *Opt. Lett.* **20** (1995) 2472–4.
89. D. B. ANDERSON and J. T. BOYD, *Appl. Phys. Lett.* **19** (1971) 266–8.
90. C. G. TREVINO-PALACIOS, G. I. STEGEMAN, M. P. DEMICHELLI, P. BALDI, S. NOUTH, D. B. OSTROWSKY, D. DELACOURT and M. PAPUCHON, *Appl. Phys. Lett.* **67** (1995) 170–2.
91. R. DANIELIUS, P. DI TRAPANI, A. DUBIETIS, A. PISKARKAS and D. PODENAS, *Opt. Lett.* **18** (1993) 574–6.
92. R. DANIELIUS, A. DUBIETIS and A. PISKARKAS, *Opt. Lett.* **20** (1995) 1521–3.

93. G. ASSANTO, Z. WANG, D. J. HAGAN and E. W. VAN STRYLAND, *Appl. Phys. Lett.* **67** (1995) 2120–2.
94. Z. WANG, D. J. HAGAN, E. W. VAN STRYLAND and G. ASSANTO, *Program for Topical Meeting on Nonlinear Optics: Materials, Fundamentals and Applications* (Opt. Soc. Am., Washington, 1996) paper NMB2.
95. L. LEFORT and A. BARTHELEMY, *Electron. Lett.* **31** (1995) 910–11.
96. L. LEFORT and A. BARTHELEMY, *Appl. Phys. Lett.* **20** (1995) 1749–51.
97. Z. WANG, D. J. HAGAN, E. W. VAN STRYLAND and G. ASSANTO, *Electron. Lett.* **32** (1996) 1135–6.
98. K. A. STANKOV, *Appl. Phys. B* **45** (1988) 191–5.
99. M. B. DANAILOV, G. CERULLO, V. MAGNI, D. SEGALA and S. DE SILVESTRI, *Opt. Lett.* **19** (1994) 792–4.
100. G. CERULLO, M. B. DANAILOV, S. DE SILVESTRI, P. LAPORTA, V. MAGNI, D. SEGALA and S. TACCHEO, *Appl. Phys. Lett.* **65** (1994) 2392–4.
101. K. A. STANKOV, *Opt. Lett.* **14** (1989) 359–61.
102. K. A. STANKOV, *Appl. Phys. Lett.* **58** (1991) 2203–4.
103. K. A. STANKOV, K. HAMAL, H. JELINKOVA and I. PROCHAZKA, *Opt. Commun.* **95** (1993) 85–6.
104. K. A. STANKOV, V. KUBECEK and K. HAMAL, *Opt. Lett.* **16** (1991) 505–7.
105. K. A. STANKOV, V. KUBECEK and K. HAMAL, *IEEE J. Quantum Electron.* **QE-27** (1991) 2135, 2141.
106. J. R. M. BARR, *Opt. Commun.* **70** (1989) 229–33.
107. C. HUO and Z. ZHU, *Opt. Commun.* **79** (1990) 328–32.
108. J. R. M. BARR, *Opt. Commun.* **81** (1991) 215–21.
109. K. A. STANKOV, V. P. TZOLOV and M. G. MIRKOV, *Opt. Lett.* **16** (1991) 639–41.
110. V. P. PETROV and K. A. STANKOV, *Appl. Phys. B* **50** (1990) 409–13.
111. K. A. STANKOV, V. P. TZOLOV and M. G. MIRKOV, *Opt. Lett.* **16** (1991) 1119–21.
112. K. A. STANKOV, V. P. TZOLOV and M. G. MIRKOV, *Appl. Phys. B* **54** (1992) 303–6.
113. S. XUE and Q. LOU, *J. Mod. Opt.* **42** (1995) 2413–24.
114. G. CERULLO, V. MAGNI and A. MONGUZZI, *Opt. Lett.* **20** (1995) 1785–7.
115. K. A. STANKOV, *Appl. Phys. B* **52** (1991) 158–62.
116. A. AGNESI, A. DEL CORNO, P. DI TRAPANI, M. FOGLEANI, G. C. REALI, J.-C. DIELS, C.-Y. YEH, XIN MIAO ZHAO and V. KUBECEK, *IEEE J. Quantum Electron.* **28** (1992) 710–19.
117. I. BUCHVAROV, S. SALTIEL, K. STANKOV and D. GEORGIEV, *Opt. Commun.* **83** (1991) 65–70.
118. J. R. M. BARR and D. W. HUGHES, *Appl. Phys. B* **49** (1989) 323–5.
119. J. R. M. BARR and D. W. HUGHES, *J. Mod. Opt.* **37** (1990) 447–54.
120. XIN MIAO ZHAO and DANIEL JOHN MCGRAW, *IEEE J. Quantum Electron.* **28** (1992) 930–8.
121. D. J. MCGRAW, Univ. New Mexico Disclosure and Record of Invention (1988) U.S. Patent 4 933 944.
122. K. A. STANKOV, *Opt. Lett.* **14** (1989) 51–3.
123. T. F. CARRUTHERS and I. N. DULING III, *Opt. Lett.* **15** (1990) 804–6.
124. Q. WU, J. Y. ZHOU, X. G. HUANG, Z. X. LI and Q. X. LI, *J. Opt. Soc. Am. B* **10** (1993) 2080–4.
125. E. IPPEN, *Appl. Phys. B* **58** (1994) 159–70.
126. RAMASWAMY, A. S. GOUVEIA-NETO, D. K. NEGUS, J. A. IZATT and J. G. FUJIMOTO, *Opt. Lett.* **18** (1993) 1825–7.
127. Y. WANG and R. DRAGLIA, *Phys. Rev. A* **41** (1990) 5645–9.
128. A. STABINIS, G. VALIULIS and E. A. IBRAGIMOV, *Opt. Commun.* **86** (1991) 301–6.
129. Y. WANG and B. LUTHER-DAVIES, *Opt. Lett.* **20** (1992) 1459–61.
130. A. UMBRASAS, J.-C. DIELS, J. JACOB, G. VALIULIS and A. PISKARKAS, *Opt. Lett.* **20** (1995) 2228–30.
131. R. DANIELUS, A. DUBIETIS, G. VALIULIS and A. PISKARSKUS, *Opt. Lett.* **20** (1995) 2225–7.
132. M. NISOLI, S. DE SILVESTRI, G. VALIULIS and A. VARANAVICIUS, *Appl. Phys. Lett.* **68** (1996) 3540–2.
133. R. LAENEN, H. GRAENER and A. LAUBEREAU, *J. Opt. Soc. Am. B* **8** (1991) 1985–8.
134. T. J. DRISCOLL, G. M. GALE and F. HACHE, *Opt. Commun.* **110** (1994) 638–44.
135. F. HACHE, A. ZEBOULON, G. GALLOT and G. M. GALE, *Opt. Lett.* **20** (1995) 1556–8.
136. M. YAMASHITA, K. TORIZUKA and T. UEMIYA, *Appl. Phys. Lett.* **57** (1990) 1301–3.
137. M. YAMASHITA, K. TORIZUKA, T. UEMIYA and J. SHIMADA, *Appl. Phys. Lett.* **58** (1991) 2727–8.
138. R. MORITA and M. YAMASHITA, *Opt. Lett.* **19** (1994) 1459–61.
139. C. R. MENYUK, *J. Opt. Soc. Am. B* **10** (1993) 1585–981.
140. A. A. KANASHOV and A. M. RUBENCHIK, *Opt. Commun.* **24** (1978) 121–4; *Physica D* **4** (1981) 122–34.
141. E. A. KUZNETSOV, A. M. RUBENCHIK and V. E. ZAKHAROV, *Phys. Rep.* **142** (1986) 103–65.
142. Q. GUO, *Quantum Opt.* **5** (1993) 133–9.
143. A. G. KALOCSAI and J. W. HAUS, *Phys. Rev. A* **49** (1994) 574–85.
144. K. HAYATA and M. KOSHIBA, *Phys. Rev. Lett.* **71** (1993) 3275–8.
145. M. J. WERNER and P. D. DRUMMOND, *J. Opt. Soc. Am. B* **10** (1993) 2390–3.

146. R. SCHIEK, Y. BAEK and G. I. STEGEMAN, *Phys. Rev. A* **53** (1996) 1138–41.
147. C. R. MENYUK, R. SCHIEK and L. TORNER, *J. Opt. Soc. Am. B* **11** (1994) 2434–43.
148. L. TORNER, C. R. MENYUK and G. I. STEGEMAN, *Opt. Lett.* **19** (1994) 1615–17; *J. Opt. Soc. Am. B* **12** (1995) 889–97.
149. L. TORNER and E. M. WRIGHT, *J. Opt. Soc. Am. B* **13** (1996) 864–75.
150. L. TORNER, C. R. MENYUK, W. E. TORRUELLAS and G. I. STEGEMAN, *Opt. Lett.* **20** (1995) 13–15.
151. M. A. KARPIERZ and M. SYPEK, *Opt. Commun.* **110** (1994) 75–9.
152. M. J. WERNER and P. D. DRUMMOND, *Opt. Lett.* **19** (1994) 613–15.
153. K. HAYATA and M. KOSHIBA, *Phys. Rev. A* **50** (1994) 675–9.
154. N. C. KOTHARI and X. CARLOTTI, *J. Opt. Soc. Am. B* **5** (1988) 756–64.
155. A. V. BURYAK and Y. S. KIVSHAR, *Opt. Lett.* **19** (1994) 1612–14; erratum **20** (1995) 1080; *Phys. Lett. A* **197** (1995) 407–12.
156. L. TORNER, *Opt. Commun.* **114** (1995) 136–40.
157. A. V. BURYAK, Y. S. KIVSHAR and V. V. STEBLINA, *Phys. Rev. A* **52** (1995) 1670–4.
158. L. TORNER, D. MIHALACHE, D. MAZILU, E. M. WRIGHT, W. E. TORRUELLAS and G. I. STEGEMAN, *Opt. Commun.* **121** (1995) 149–55.
159. S. TRILLO and P. FERRO, *Phys. Rev. E* **51** (1995) 4994–8.
160. A. V. BURYAK and Y. S. KIVSHAR, *Opt. Lett.* **20** (1995) 834–6.
161. A. V. BURYAK and Y. S. KIVSHAR, *Phys. Rev. A* **51** (1995) 41–4.
162. D. MIHALACHE, F. LEDERER, D. MAZILU and L.-C. CRASOVAN, *Opt. Eng.* **35** (1996) 1616–23.
163. H. HE, M. J. WERNER and P. D. DRUMMOND, *Phys. Rev. E* **54** (1996) 896–911.
164. A. V. BURYAK, *Phys. Rev. E* **52** (1995) 1156–63.
165. Y. S. KIVSHAR, *Phys. Rev. E* **51** (1995) 1613–15.
166. L. TORNER, D. MAZILU and D. MIHALACHE, *Phys. Rev. Lett.* **77** (1996) 2455–80.
167. C. ETRICH, U. PESCHEL, F. LEDERER, B. MALOMED and Y. S. KIVSHAR, *Phys. Rev. E* (1996) to be published.
168. L. BERGE, V. K. MEZENTSEV, J. J. RASMUSSEN and J. WYLLER, *Phys. Rev. A* **52** (1995) 28–31.
169. S. K. TURITSYN, *JETP Lett.* **61** (1995) 469–72.
170. D. E. PELINOVSKY, A. V. BURYAK and Y. S. KIVSHAR, *Phys. Rev. Lett.* **75** (1995) 591–5.
171. L. TORNER, D. MIHALACHE, D. MAZILU and N. N. AKHMEDIEV, *Opt. Lett.* **20** (1995) 2183–5.
172. A. D. BOARDMAN, K. XIE and A. SANGARPAUL, *Phys. Rev. A* **52** (1995) 4099–106.
173. N. AKHMEDIEV, A. BURYAK and J. M. SOTO-CRESPO, *Opt. Commun.* **112** (1994) 278–82.
174. K. HAYATA and M. KOSHIBA, *J. Opt. Soc. Am. B* **12** (1995) 2288–95.
175. B. A. MALOMED, D. ANDERSON, A. BERNTSON, M. FLORJANCYK and M. LISAK, *Pure and Appl. Opt.* (1996) to be published.
176. H. HE, P. D. DRUMMOND and B. A. MALOMED, *Opt. Commun.* **123** (1996) 394–402.
177. S. TRILLO, A. V. BURYAK and Y. S. KIVSHAR, *Opt. Commun.* **122** (1996) 200–11.
178. A. V. BURYAK, Y. S. KIVSHAR and S. TRILLO, *Opt. Lett.* **20** (1995) 1961–3.
179. M. A. KARPIERZ, *Opt. Lett.* **20** (1995) 1677–9.
180. C. R. MENYUK, *Opt. Lett.* **12** (1987) 614–16; *J. Opt. Soc. Am. B* **5** (1988) 392–402.
181. M. N. ISLAM, *Ultrafast Fiber Switching Devices and Systems* (Cambridge University Press, Cambridge, 1992).
182. L. TORNER, W. E. TORRUELLAS, G. I. STEGEMAN and C. R. MENYUK, *Opt. Lett.* **20** (1995) 1952–4.
183. W. E. TORRUELLAS, Z. WANG, L. TORNER and G. I. STEGEMAN, *Opt. Lett.* **20** (1995) 1949–51.
184. W. E. TORRUELLAS, G. ASSANTO, B. L. LAWRENCE, R. A. FUERST and G. I. STEGEMAN, *Appl. Phys. Lett.* **68** (1996) 1449–51.
185. G. LEO, G. ASSANTO and W. E. TORRUELLAS, *Opt. Commun.* (1996) to be published.
186. L. TORNER, J. P. TORRES and C. R. MENYUK, *Opt. Lett.* **21** (1996) 462–6.
187. A. B. ACEVES and S. WABNITZ, *Phys. Lett. A* **141** (1989) 37–42.
188. J. M. SOTO-CRESPO, N. AKHMEDIEV and A. ANKIEWICZ, *Phys. Rev. E* **51** (1995) 3547–55.
189. D.-M. BABOIU, G. I. STEGEMAN and L. TORNER, *Opt. Lett.* **20** (1995) 2282–4.
190. C. ETRICH, U. PESCHEL, F. LEDERER and B. MALOMED, *Phys. Rev. A* **52** (1995) 3444–7.
191. C. B. CLAUSEN, P. L. CHRISTIANSEN and L. TORNER, *Opt. Commun.* (1996) to be published.
192. D. J. KAUP, A. REIMAN and A. BERS, *Rev. Mod. Phys.* **51** (1979) 275–309.
193. V. E. ZAKHAROV and S. V. MANAKOV, *Sov. Phys. JETP* **42** (1976) 842–50.
194. D. J. KAUP, *Physica D* **3** (1981) 374–95.
195. F. CALOGERO, *J. Math. Phys.* **30** (1989) 28–40.
196. R. FUERST, B. LAWRENCE, W. TORRUELLAS and G. I. STEGEMAN, *Technical Digest for QELS'96* (Opt. Soc. Am., Washington, 1996) p. 179, paper QthE2.